



**ACCURATE DYNAMIC RESPONSE PREDICTIONS OF
PLUG-AND-PLAY SAT I**

THESIS

Michael D. Trottier, 2d Lt, USAF

AFIT/GA/ENY/10-M12

**DEPARTMENT OF THE AIR FORCE
AIR UNIVERSITY**

AIR FORCE INSTITUTE OF TECHNOLOGY

Wright-Patterson Air Force Base, Ohio

APPROVED FOR PUBLIC RELEASE; DISTRIBUTION UNLIMITED

The views expressed in this thesis are those of the author and do not reflect the official policy or position of the United States Air Force, Department of Defense, or the United States Government. This material is declared a work of the U.S. Government and is not subject to copyright protection in the United States.

AFIT/GA/ENY/10-M12

**ACCURATE DYNAMIC RESPONSE PREDICTIONS
OF PLUG-AND-PLAY SAT I**

THESIS

Presented to the Faculty

Department of Aeronautics and Astronautics

Graduate School of Engineering and Management

Air Force Institute of Technology

Air University

Air Education and Training Command

In Partial Fulfillment of the Requirements for the
Degree of Master of Science in Astronautical Engineering

Michael D. Trottier, BS

2d Lt, USAF

March 2010

APPROVED FOR PUBLIC RELEASE; DISTRIBUTION UNLIMITED

**ACCURATE DYNAMIC RESPONSE PREDICTIONS
OF PLUG-AND-PLAY SAT I**


Michael D. Trottier, BS

2d Lt, USAF

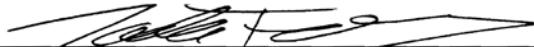
Approved:



Lt Col Eric D. Swenson, USAF (Chairman)



Dr. Richard Cobb (Member)



Dr. Jonathan T. Black (Member)

18 Feb 10

Date

19 MAR 10

Date

19 MAR 2010

Date

Abstract

Researchers at the Air Force Institute of Technology (AFIT) and the Operationally Responsive Space (ORS) Office have conducted extensive vibration testing and structural modeling on the first ORS Plug-and-Play Satellite (PnPSAT I). The intent of this research effort is to evaluate the premise that current post-integration spacecraft environmental test requirements can be reduced or modified using accurately tuned finite element (FE) models. As part of this research, modal testing was conducted on the PnPSAT I structural panels at AFIT. The modal testing was part of a much larger series of experimental trials on various configurations of PnPSAT I at the Air Force Research Laboratory (AFRL) facilities at Kirtland Air Force Base (KAFB). Multiple sets of vibration data were also collected from accelerometers on PnPSAT I from standard and modified spacecraft prelaunch sine sweep and random vibration tests. The modal data collected at AFIT is used to tune two PnPSAT I panel FE models and the random vibration data collected at KAFB is used to tune the complete satellite for one configuration. The goal is to create an accurate FE model capable of predicting the dynamic response in a frequency range of 0-300 Hz of various PnPSAT configurations. This modeling and tuning effort will be validated by comparing FE model predictions with measured vibrational response from the previously mentioned experimental trial.

Acknowledgements

Special thanks to my thesis advisor Lt Col Eric Swenson for allowing me to utilize a lot of his time. He has been a mentor and a guide for the entirety of this thesis and his help was invaluable. Thanks to my committee members Dr. Jonathan Black and Dr. Richard Cobb for their feedback. Thanks to Lisa Baghal for offering a helping hand in answering any questions. Thanks to Rob Fievisohn, Mike Vinacco, Ben Switzer, and Joe Sabat for making the linux lab bearable after hours.

Table of Contents

Abstract	iv
Acknowledgements	v
Table of Contents	vi
List of Figures	viii
<i>List of Abbreviations</i>	xiii
I. Introduction	1
1.1 ORS and PnP Test Program	2
1.2 Overall Rapid AI&T Program	4
1.3 Finite Element Modeling	5
1.4 Research Overview	7
1.5 Thesis Organization	9
II. Background	10
2.1 Eigenanalysis and FE Model Tuning References	10
2.2 Finite Element Analysis	14
2.3 Modal Analysis	15
2.4 Scanning Laser Vibrometer Data Collection Fundamentals	17
2.5 Finite Element Model Tuning	22
III. Method	26
3.1 Method Overview	26
3.2 Generate -Y and -Z Panels FE Models	26
3.3 Test Setup	32
3.4 Mode Shape Extraction	40
3.5 Tuning -Y and -Z panels	42
3.6 Creating Entire PnPSAT I Using -Y and -Z panel	44
3.7 Measurement Method for Frequency data for Entire PnPSAT I	48
3.8 Tuning PnPSAT I	51
IV. Results and Discussion	52
4.1 Untuned -Y and -Z panel FE model Results	52
4.2 Tuned -Y and -Z panel FE model Results	56
4.3 Untuned PnPSAT I	63

4.4 <i>Tuned PnPSAT I</i>	68
V. Conclusion.....	71
5.1 <i>Research Overview</i>	71
5.2 <i>Future Work</i>	74

List of Figures

Figure 1: PnPSAT fully configured ready for test.	2
Figure 2: The three tiers of the ORS Office <i>Bhopale</i> [2009].	3
Figure 3: Fully deployed high fidelity model of PnPSAT I.	6
Figure 4: (a) Spaceworks high fidelity PnPSAT I model. (b) close-up view in top of Z panel showing rigid links (dark thick lines), represented by point masses with links, these links connect to the point masses representing the components to the satellite's panel.	6
Figure 5: Overall process for creating and tuning PnPSAT I FE model.	8
Figure 6: 3 Head Scanning Laser Vibrometer	19
Figure 7: Frequency Response Function of $-Z$ panel	23
Figure 8: Picture of one half of PnPSAT I $-Y$ panel with electrical components; arrows point out the unique ribbed structure which joins the two halves of the panel together.	28
Figure 9: CAD geometry model of the $-Z$ panel.	29
Figure 10: Nodal representation of the $-Z$ panel.	29
Figure 11: $-Z$ Panel FE Model where, each color represents a different material card (95 total); these material card's properties are altered in the tuning process.	30
Figure 12: Transparent $-Z$ panel showing the spring dampers (black) in the corners with fixed node constraint. Elevates rigid body mode to avoid singular mass and stiffness matrices... 31	31
Figure 13: Test harness.	33
Figure 14: PnPSAT $-Y$ panel with precise nodes and arbitrary points, reflective tape located on corners.	34
Figure 15: MB Dynamics Cal50 exciter electrodynamic shaker, setup to perform as an automatic ping hammer.	34

Figure 16: Coherence of testing on the $-Z$ panel.....	35
Figure 17: (a) Shaker striking points on bottom side of panel (tested facing other direction) (b) picture of the fifth mode, dark regions represent nodal lines.....	36
Figure 18: Spectral density plot of an impact excitation <i>Doupe</i> [2009].....	37
Figure 19: Top Left: A good impact excitation. Top Right: A squared-off peak on pulse indicates that the hammer struck the test article too slowly. An adjustment of the pulse width is necessary. Bottom Left: The striker hits the panel multiple times indicating both frequency and magnitude needs to be adjusted. Bottom Right: Side lobes indicate that the magnitude is too high <i>Doupe</i> . [2009].....	38
Figure 20: Typical node points on the $-Z$ panel from PSV. Points picked from FE model to avoid holes and scratches. Blue means unmeasured, green means successful measurement and gray means over ranging typically caused due to people talking or walking around the room.	39
Figure 21 (a) Satellite panel in test stand and (b) PSV-400-3D LDV.	40
Figure 22: PnPSAT I panels open and joined together via hinges.	44
Figure 23: (a) Adapter ring modeled with plate elements, constraint forces attached (b) base plate acquired from Spaceworks model.	45
Figure 24: (a) Demonstration of coincident nodes (b) constructed PnPSAT I (c) side view of the spring elements connecting the adapter ring to the base plate.	46
Figure 25: Look into PnPSAT I FE model showing interior components attached via rigid links.	47
Figure 26: Complete PnPSAT I model with components connected by rigid links.	48
Figure 27: PnPSAT I on the vibration table on Kirtland AFB.	49

Figure 28: (a) FRF of Sine sweep from 0 to 2000 Hz on X Axis test (b) FRF of random vibration sweep from 0 to 2000 Hz on X Axis Test, green represents input and black represents output.	50
Figure 29: Measured versus analytical mode shapes –Y panel.	54
Figure 30: Measured versus analytical mode shapes –Z panel.	55
Figure 31: -Z Panel (a) Unsatisfactory objective function, single value approaching 300, tuned mode divided by small erroneous data (b) Removed bad data points all points with +/- 3 magnitude – note the y-axis scale difference.	56
Figure 32: (a) -Z panel, 130 nodes (b) -Y panel, 137 nodes.	57
Figure 33: (a) -Y panel tuned cross-orthogonality results (b) -Y measured vs. measured cross-orthogonality (c) -Z panel tuned cross-orthogonality results (d) -Z measured vs. measured cross-orthogonality.	59
Figure 34: (a) Modulus of Elasticity of the various tuning variables the –Y Panel. Initial value of 9.9E6 Ksi. (b) Elements with 5.90E6 modulus of elasticity. (c) Elements with modulus of elasticity between 5.90E6 Ksi and 1.30E7 Ksi. (d) Elements with modulus of elasticity of 1.30E7 Ksi.	61
Figure 35: (a) Modulus of Elasticity of the various tuning variables the –Z Panel. Initial value of 9.9E6 Ksi. (b) Elements with 3.50E6 modulus of elasticity. (c) Elements with modulus of elasticity between 3.50E6 Ksi and 1.60E7 Ksi. (d) Elements with modulus of elasticity of 1.60E7 Ksi.	62
Figure 36: Blown up view between base plate and adapter ring, primary strain along top of adapter ring	64

Figure 37: Mode 1: Rocking X: untuned 63.2 Hz: (a) undeformed dimetric view (b), (c) scaled up deflections demonstrating the rocking motion.	65
Figure 38: Mode 2: Rocking Y: untuned 70.6 Hz (a) undeformed dimetric view (b), (c) scaled up deflections demonstrating the rocking Y mode.	66
Figure 39: Mode 3: Pogo mode untuned 158.9 Hz (a) undeformed dimetric view (b), (c) scaled up deflections demonstrating the pogo mode.....	67
Figure 40: (a) Modulus of Elasticity of the various tuning variables the –Y Panel. Initial value of 9.9E6 Ksi. (b) Elements with 5.90E6 modulus of elasticity. (c) Elements with modulus of elasticity between 5.90E6 Ksi and 1.30E7 Ksi. (d) Elements with modulus of elasticity of 1.30E7 Ksi.....	69
Figure 41: Spring Stiffness Coefficients: Includes both axial and torsional spring values. The initial starting parameter value was 1.0E3 lbf/in (axial) or 1.0E3 lbf in/rad (torisonal).	70

List of Tables

Table 1: Comparison between actual and model mass.	52
Table 2: Comparison between Spaceworks and newly created untuned –Y and –Z FE models..	52
Table 3: Material cards –Z, -Y panels.	56
Table 4: Measured versus tuned for modes 1-6 for –Y panel.	58
Table 5: Measured versus tuned for modes 1-6 for –Z panel; ordered by analytical modes.	58
Table 6: Table comparing untuned and tuned cross orthogonality checks –Z panel.	60
Table 7: Table comparing untuned and tuned cross orthogonality checks –Y panel.	60
Table 8: Comparison of size of Spaceworks and reduced PnPSAT I FE models.	63
Table 9: Experimental vs. tuned natural frequencies for modes 1-3.	68

List of Abbreviations

AFIT – Air Force Institute of Technology
AIT – Assembly, Integration, and Test
ASTROS – Automated Structural Optimization System Software
CAD – Computer Aided Design
C.G. – Center of Gravity
DFT – Discrete Fourier Transform
DOF – Degree of Freedom
EOM – Equations of Motion
ERA – Eigensystem Realization Algorithm
EVP – Eigen-Value Problem
FEMAP – Finite Element Model Analysis Program
FFT – Fast Fourier Transform
FRF – Frequency Response Function
FS5 – Falcon SAT 5
GUI – Graphical User Interface
LDV – Laser Doppler Vibrometry
MOI – Moment of Inertia
ODS – Operational Deflection Shape
ORS – Operationally Responsive Space
PC – Personal Computer
PnP – Plug and Play Satellite
SPA – Space Plug-n-Play Avionics
TVac – Thermal Vacuum
USB – Universal Serial Bus

ACCURATE DYNAMIC RESPONSE PREDICTIONS OF PNPSAT I

I. Introduction

Satellites are very complex systems that must meet intensive and strict design, manufacture, test, and integration requirements for a successful mission. Rigorous post-integration acceptance tests are critical to guard against failures during launch and deployment. Presently, post-integration satellite environmental tests, such as vibration and thermal vacuum (TVac), typically exceed several months in duration for traditional satellites Wertz [1999], Yee [2005]. However, Plug-and-Play (PnP) satellites are designed to fulfill rapid, time sensitive mission requirements. Because satellites are typically very expensive, traditional satellites are mostly designed as a one-of-a-kind flight articles and its components are ordered or built in as-required quantities. Confidence in the fully-integrated satellite is only gained through exhaustive pre-flight acceptance tests. Conversely, PnP satellites are constructed from a wide array of known components and are designed to minimize integration issues. Like components on traditional satellites, all PnP components will have passed individual and possibly subsystem operational acceptance tests. Prior to satellite construction, after the components have been selected for flight, additional and possibly exhaustive environmental tests, including hardware and software, are typically conducted to significantly increase confidence in the fully-integrated satellite.

These environmental tests are necessary to ensure that the satellite is certified flight-ready and that no issues or anomalies are overlooked. In general, all flight hardware is exhaustively tested in order to certify that it can survive launch and operate in the space environment. In order to reduce risk, full assembly integration and test (AIT) program is conducted on each level of assembly ranging from components and subsystems to the entire satellite. However, traditional timelines to complete post-integration vibration and TVac tests must be reduced for

PnP satellites to be launched in days as opposed to months. In order to determine if test processes can be reduced or modified while maintaining high reliability, AFIT and ORS researchers are conducting experiments to evaluate traditional acceptance tests, reduced, and new acceptance tests on a fully-integrated satellite, this set of experiments is also referred to as the Rapid AI&T Demonstration.

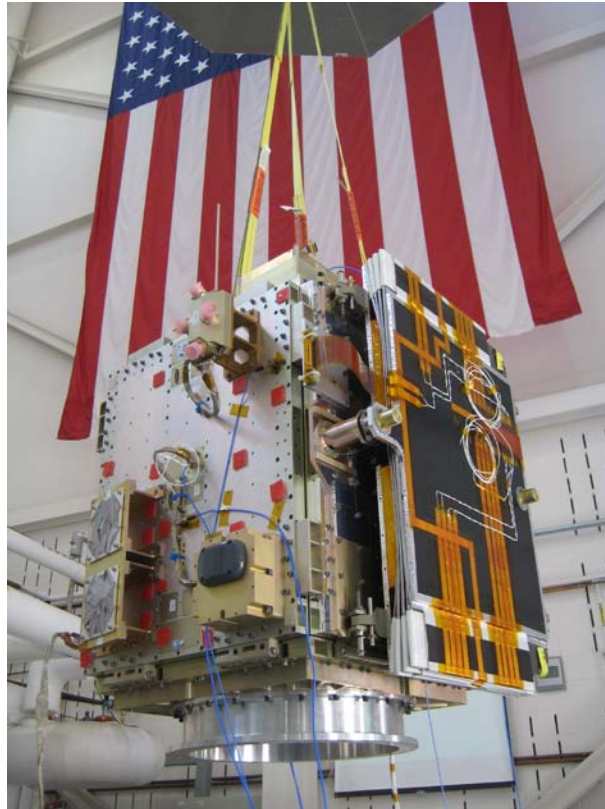


Figure 1: PnPSAT fully configured ready for test.

1.1 ORS and PnP Test Program

The ORS office is responsible for the development of capabilities that provide assured space power focusing on timely mission constraints in order to satisfy the Joint Force Commanders' needs by employing, deploying, or developing new systems to sustain or augment capabilities

Bhopale [2009]. ORS consists of three distinct tiers each responsible for a different task, these tiers are shown in Figure 2.

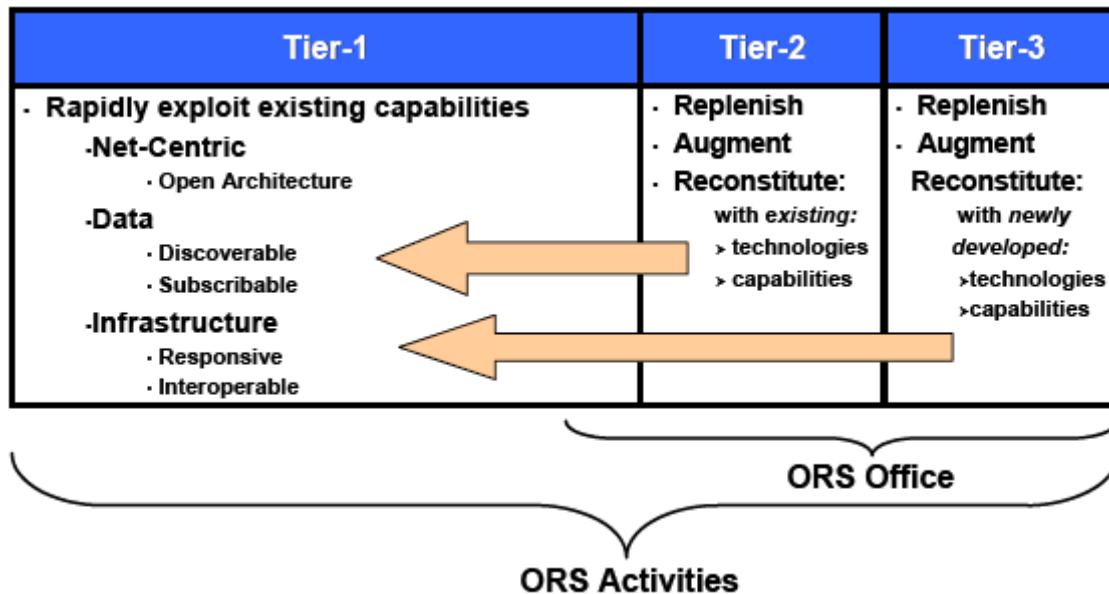


Figure 2: The three tiers of the ORS Office *Bhopale* [2009].

Tier-1 is comprised of capabilities readily available that provide highly responsive space effects. Therefore, these solutions utilize existing space systems, ground systems, operations and processes and typically are employed within a few hours-to-days. If Tier-1 is unachievable a Tier-2 solution is considered. Tier-2 solutions utilize field-ready capabilities which exist in the days-to-weeks time frame. Consequently Tier-3 exists to create technologies that will eventually be classified as Tier-2 once they are field ready. For a more detailed description of ORS refer to *Bhopale* [2009]. PnPSAT I falls into the Tier-2 classification, PnPSAT I is meant to be fully assembled and ready for mission within 6 days of being called upon.

Since the beginning of satellite assimilation and deployment, satellite design has been an extremely non-standardized and complex process. Usually, highly experienced personnel are required to synthesize, create, build, test, and launch a satellite. Like the advent of the personal

computer (P C) with the invention of universal serial bus (USB), strides have been taken to simplify the way satellites are constructed. The Air Force Research Lab, Space Vehicles Directorate (ARFL/RV) has undertaken two efforts in small satellite development to demonstrate the effectiveness of the technology and show it is beneficial. The first effort, PnPSAT I utilizes the space Plug-n-Play avionics (SPA) interface standard. Implementation of this SPA interface standard has proven that rapid development, integration and test is possible. In the second effort, PnPSAT II uses the next generation of SPA components for a larger bus focused on ORS needs to ensure custom performance at commodity prices. In short, all the components exist and are meant to be like the name suggests, Plug-n-Play, similar to the PnP standard for PCs. The idea is that the user can plug components into the satellite using standard connectors across all components and quickly assemble, test, and launch a satellite in order to replenish or populate a constellation to conduct a mission. The predicted timeline for ORS Tier-2 satellites allows only a three day window for integration of testing (Rapid AIT). Consequently, leaving only two days to fully integrate and launch the satellite.

As part of the aforementioned Rapid AIT, it is important to minimize vibration and thermal testing. These expensive tests are manpower and time consuming; elimination or at least a reduction of these tests is of critical importance to the ORS mission. The overall test program for reducing these post-integration is described below.

1.2 Overall Rapid AI&T Program

The Rapid AIT demonstration is designed to explore the premise that current spacecraft test requirements can be reduced or modified for ORS PnP satellites by modifying processes, testing strategies, and personnel dependencies *Baghal* [2010]. There are four trials in the Rapid AI&T

Demonstration plan. Each trial is designed to investigate one variables' dependency on that same variable. For example, in Trials 1 & 2, the only difference is the personnel performing the assembly and test. The two groups were referred to as Team A and Team B. Team A consisted of personnel intimately familiar with PnPSAT. Team B consisted of spacecraft technologists that are not familiar with PnPSAT specifically. Team B trained during Trial 1 and performed the assembly and test on Trial 2. The updates to AI&T flow and/or spacecraft configuration for Trials 3 and 4 will be determined upon an assessment from Trials 1 and 2.

After each PnP satellite disassembly and reassembly, traditional acceptance tests, reduced, and new acceptance tests are conducted on the components and/or subsystems. Dynamic and thermal models are correlated with the collected data and predictions will be made on the response of the fully-integrated satellite. Later tests include various configurations in order to determine to the capability of models to predict responses of various configurations. After the data is analyzed, the results may indicate that post-integration tests can be reduced while incurring little increase in risk.

1.3 Finite Element Modeling

In order to further reduce rigorous post-integration testing, a finite element (FE) model of PnPSAT I was created by Spaceworks. The FE model was created from a CAD model from which the satellite was made from. This CAD model is extremely accurate because it includes even the finer details such as every bolt, washer and screw, as seen in Figure 3. From this CAD model, the mass moments of inertia (MOI) of the satellite can be estimated which are used primarily for launch vehicle integration.

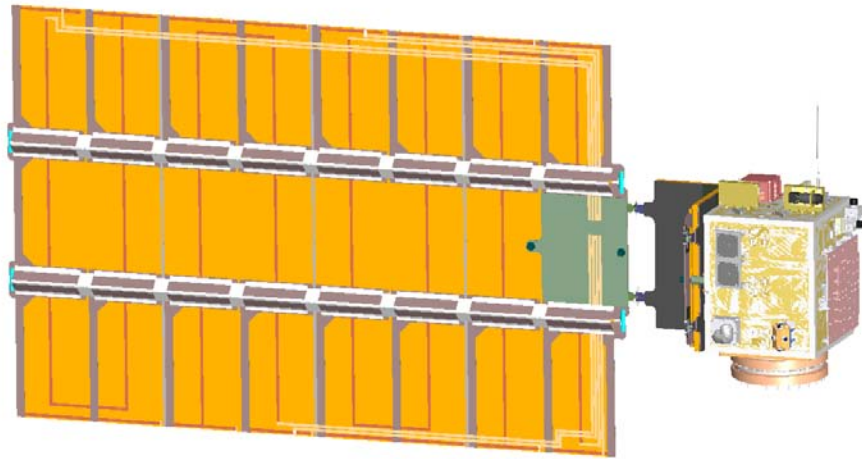


Figure 3: Fully deployed high fidelity model of PnPSAT I.

Spaceworks, the company that created the original CAD model was tasked to create an FE model of PnPSAT I. Their FE model was used to predict the structure's natural frequencies. The FE model has 368,850 nodes and 246,295 elements and 1,104,633 DOF, see Figure 4.

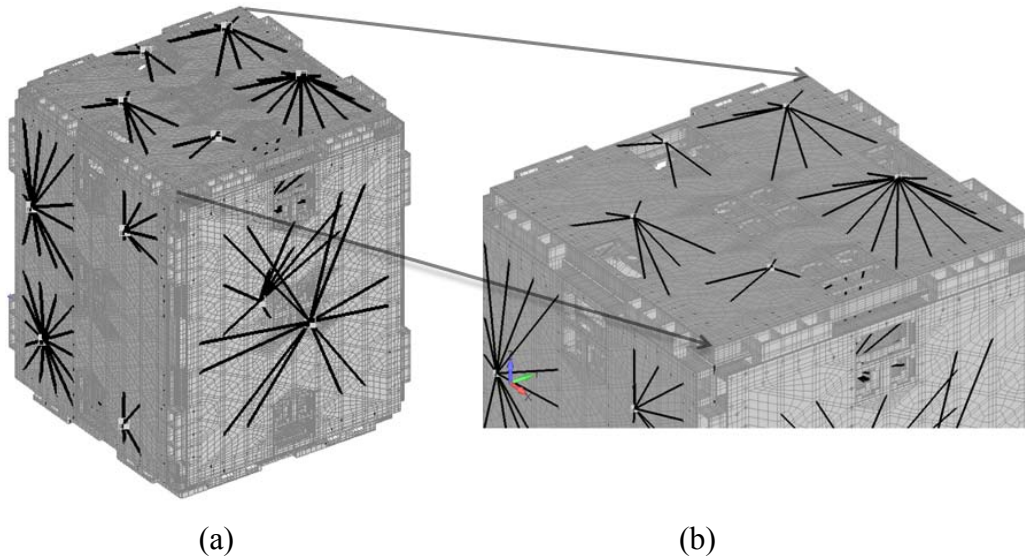


Figure 4: (a) Spaceworks high fidelity PnPSAT I model. (b) close-up view in top of Z panel showing rigid links (dark thick lines), represented by point masses with links, these links connect to the point masses representing the components to the satellite's panel.

The Spaceworks FE model, although very refined, has too many FE DOF for tuning in a reasonable amount of time. Tuning involves minimizing the difference between analytical and measured modes while constraining the natural frequencies. In order to tune PnPSAT I, a new FE model with significantly fewer elements needed to be created. Like the Spaceworks FE model, the Spaceworks CAD model served as the starting point for the new reduced FE model, development and tuning is the focus of this research.

1.4 Research Overview

The PnP concept on which PnPSAT I was initially conceived was aimed at the elimination or reduction of expensive and time consuming AIT. The ORS mission is to launch payloads to space in less than six days. The objective of this research is to investigate the possibility of creating accurate FE models to model PnPSAT I in order to predict its natural frequencies in different configurations. This would eliminate the amount of vibration testing required making it possible to launch in six days.

The process is initialized by generating FE models of both PnPSAT I's -Y and -Z panels (only two panels were required for modal testing). The FE models possess the very similar geometry and mass as the actual panels of the satellite. Next, modal data is extracted from the impulse response from both the -Y and -Z panels. The FE models are then tuned using the collected modal data by only changing the panels modulus of elasticity. As a result, the tuned FE model panels are copied and combined to create the main structure of the PnPSAT I. PnPSAT I FE model structure is rigidly attached via coincident nodes, the components are attached to match the first test configuration in the Rapid AIT Demonstration. This complete satellite FE model is

tuned using only natural frequency data collected at one of the previously mentioned K AFB shaker tests.

A flow chart of this tuning process implemented in this research is in Figure 5.

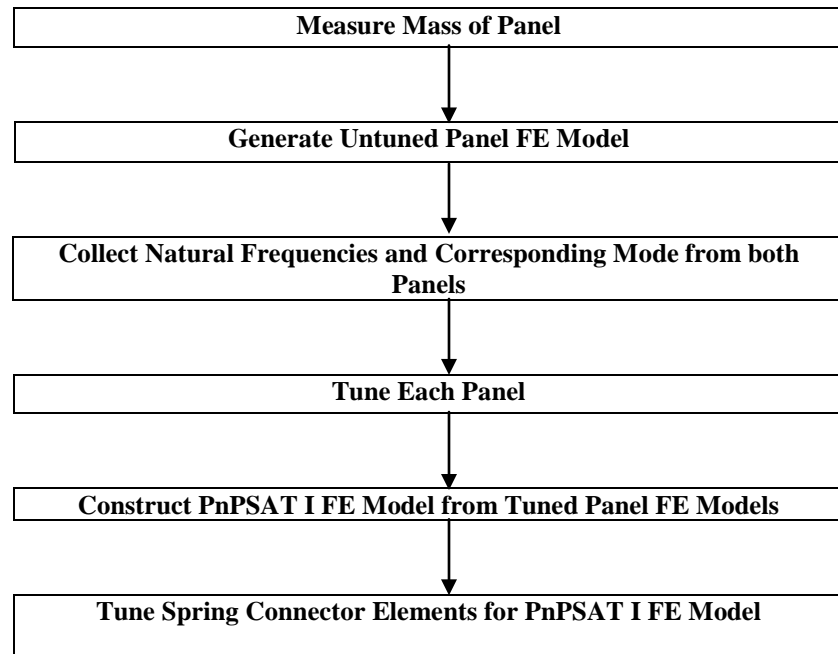


Figure 5: Overall process for creating and tuning PnPSAT I FE model.

1.5 Thesis Organization

The second of five chapters provides a literature review of previous efforts to tune satellite FE models, technical background behind FE modeling/analysis, collecting modal data, and the optimization process. The third chapter describes the methods used to create the FE model, the collection of modal data, and tuning the models. Chapter Four provides the results of the modal analysis to include untuned, tuned models and the comparison of results between different configurations and experimental data. The final chapter concludes with a discussion on the conclusions drawn from the results and recommendations for any future work.

II. Background

The following chapter provides details into the FE model. The first section provides a literature review of FE modeling and tuning processes. The second section describes FE analysis to include how to generate a FE model and the assumptions used. Third, eigenanalysis is described starting from the equations of motion (EOM) through the eigenvalue problem (EVP) ultimately leading to the modal frequency response problem. The next section details the scanning laser vibrometer used to collect the panel impulse responses at hundreds of points to include a discussion on how the software works. Lastly, the overall process for tuning the FE model with the acquired modes and natural frequencies is discussed.

2.1 Eigenanalysis and FE Model Tuning References

Eigenanalysis and FE model tuning has been a necessity in the space launch arena for sometime. An innovative approach was taken by *Cobb* [1996] in his attempt to model and tune a 6-m flexible frame structure from 0 to 70Hz. Although a different structure, a similar process was used to tune this model. The same objective function as presented later,

$$J = \sum_{i=1}^p a_i \left[1 - \left| \frac{\lambda_i}{\hat{\lambda}_i} \right| \right]^2 + \sum_{i=1}^p \sum_{j=1}^r b_i \left[1 - \left| \frac{\bar{\phi}_{ij}}{\hat{\phi}_{ij} \hat{\phi}_{iN}} \right| \right]^2 \quad (1)$$

was utilized, along with the same mode tracking process. Different software was utilized to implement the process, ASTROS (Automated Structural Optimization System Software) versus NASTRAN. The structure's measured data was taken with accelerometers reading only one direction and the input excitation to the truss was two linear momentum exchange actuators. Mounting plates were developed to attach the excitation devices atop two longerons on the free

end of the truss. Driving the actuators in phase allowed for measurement of the bending modes in one axis. The torsional modes were excited by driving the two 180 deg out of phase.

The FE model was comprised of four different types of beam elements for a total of 100 elements. Similar to the components in PnPSAT I FE model, the actuators and mounting plate were modeled as lump masses and therefore, included in the dynamics. The vibration test was conducted using 0 -100 Hz random noise sequence. Frequency averaged transfer functions between the input excitation and the eight accelerometers were measured. The inverse discrete Fourier transform of these yielded the impulse response functions which were input into an eigensystem realization algorithm (ERA). ERA is based on extracting a state-space model from the impulse response of a system. For a more detailed look at this method refer to *Juang and Pappa* [1985]. ERA extracted modes and natural frequencies from the experimental data.

Using this measured data the FE model was tuned using ASTROS and various Fortran 77 subroutines created for eigenvector normalization, mode switching, eigenvalue and eigenvector sensitivities, objective function evaluation and processing data to and from the optimization modules. The final results of the method showed the potential of this process and it was a good baseline for any FE model tuning. Overall, the same tuning process was utilized, and the differences arose between the methods of collecting and processing the data, and the software used to tune.

A unique approach was used by *Kammer* [1999] in studying the structural integrity of Russia's Mir space station. Mir provided a rare opportunity to evaluate methods of detecting structural damage on a structure currently on orbit. Modal identification was used to gather data on the potential damage on Mir; however, it provided a formidable challenge for several reasons. Mir modal data was taken during short time duration docking events; also, it was coupled with the

availability of only a few data sets which excluded the effectiveness of averaging. In addition, due to the docking element it makes the problem nonlinear making the use of ERA unsuitable for this problem. Typically, during a modal test, the input and output are measured from a pulse, and frequency response functions are generated. Many methods are applicable for modal identification. However, for Mir, the input, ships docking, were not measured making common practices void. The method investigated to solve the challenges involved with the Mir was the inverse system identification technique. This approach initially presented by *Kammer* [1999] identifies the vibrational characteristics of an inverse representation. An inverse representation differs from a normal system representation in that the input and output are switched. Meaning, the changes in the natural frequencies and modes directly relate to the system parameters of the structure, for a more detailed look refer to *Kammer et al.* [1999]. A 2646 DOF FE model of Mir was utilized to match the analytical output to the measured. From this the input was derived and more thorough tests on the structural health of Mir were conducted.

The largest interplanetary spacecraft ever developed, Cassini, launched on a Titan-IV, Centaur launch vehicle required a test verified finite element model to be completed and approved by NASA. The validation of the model was critical to final verification of coupled loads analysis and margin of safety assessments, *Coleman et al.* [1996]. Modal data was taken using a static test and component sine sweep tests to be used to verify the FE model. Before testing could occur, an FE model with a correct mass and configuration was used to determine shaker location and assess instrumentation location. The FE model Guyan-reduced mass matrix from the FE model was used for orthogonality and effective mass calculations. The analytical approach used to correct the FE model was the eigenvalue problem, this method allows for the variation of many modal parameters to ensure a verified model. The objective function

represented below was different because it was based primarily on frequencies; they were stressed to be the most important.

$$e = \sum_{pairs_{j,k}} W_{j,k}^F (f_j^A \bullet f_k^T)^2 + \sum_{pairs_{j,k}} W_{j,k}^X (X_{jk} \bullet X_{jk}^\bullet)^2 \quad (2)$$

where $W_{j,k}^F$ and $W_{j,k}^X$ are diagonal weighting matrices for frequency and cross orthogonality, with nonzero values at matching test mode pairs. Also, f_j^A and f_k^T are the analytical and test frequencies, X_{jk} is the cross orthogonality matrix between analytical modes j and test modes k . X_{jk}^\bullet is the desired cross orthogonality matrix. Optimal model parameters were achieved by driving this error function e down to zero by updating model idealizations, joint flexibilities and stiffness.

The tuning approach that most closely resembles the method used to tune PnPSAT I was developed by *Doupe et al.* [2009]. They created FE models of the panels of Falcon SAT 5 (FS5), experimentally collected natural frequencies and modes using a scanning laser vibrometer of the impulse response of each panel. Every panel FE model was tuned and then a full FS5 model was created by connecting the panels together by spring/damper elements. Next, the impulse response was collected for the fully constructed FS5 and was used to tune the completed FS5 FE model. The advantage of this process was the actual satellite and all its components were available to be taken apart and tested. Therefore, all masses could be measured making modeling the mass more certain. Another advantage of possessing the entire satellite is that it is possible to gather not only the natural frequencies but also the lower frequency modes of the constructed satellite. This allows the objective function to minimize the difference between the

modes while maintaining fixed natural frequency constraints leading to an accurately tuned complete FE model for 0-300 Hz for five modes.

2.2 Finite Element Analysis

FE analysis is a numerical process involving solution of field problems *Cook et al.* [2002]. The field values are any dependent variables described by differential or integral equations. FE codes reformulate differential or integral equations into algebraic ones using interpolation functions and solve them at discrete points called nodes. Each node is connected to other nodes through elements. Elements can be composed of various geometric shapes from a one-dimensional to a three-dimensional element. An arrangement of elements creates a mesh which represents the structure. In creating an FE model, many common assumptions are made to avoid over complication of the FE functions mesh. First, complex geometric shapes like isogrid panels, hinges and components are usually simplified to simpler shapes such as squares and rectangles. In the case of the PnPSAT I model, most of the connectors such as screws, nuts and bolts are not directly modeled to reduce model complexity. Second, materials are assumed homogenous, meaning they possess the same material properties throughout. PnPSAT I is predominantly an all aluminum structure. Third, materials are assumed isotropic and constant meaning they have the same properties in every direction and their properties do not change. Small displacements and rotations are assumed along with fixed loads and boundary conditions. All linear assumptions apply with respect to material properties, geometry, and loads.

The FE analysis process generally involves three steps: pre-processing, numerical analysis, and post-processing. Pre-processing involves creating an FE model of the test article to include choosing element types, material properties, loads, boundary conditions, and mesh density.

Next, an eigenanalysis is completed which acquires the modes and natural frequencies. Finally, post-processing is performed to analyze the computed analytical results.

2.3 Modal Analysis

Modal analysis is used to measure the dynamic response of PnPSAT I to various loads. Modal analysis is the process of measuring the three dynamic characteristics of structures: modes, damping ratios, and natural frequencies. A mode is the magnitude-independent vector representation of the shape of a structure when the structure is resonating at a natural frequency. Damping involves any mechanism that removes energy from a structure. For example, a shock absorber is a classic example of a viscous damper. Natural frequencies, also known as resonant frequencies, are the frequencies in which the structure has a tendency to oscillate at larger amplitudes.

The discrete FE equations of motion (EOM) for complex structures can be written in the time domain as:

$$M \ddot{\bar{x}}(t) + (1 + i\gamma)K \bar{x}(t) = F(t) \quad (3)$$

where $M \in \mathbb{R}^{n \times n}$ represents the mass matrix, $K \in \mathbb{R}^{n \times n}$ represents the stiffness matrix and γ is the structural damping coefficient. Both M and K matrices are symmetric. The reduced PnPSAT I FE model developed in this research has over 40,000 elements and 70,000 nodes. Each node possesses either three or six DOFs making $n \approx 200,000$. $F(t)$ represents the force matrix and is $F \in \mathbb{R}^{n \times m}$ which can have tens to hundreds of load cases. Because PnPSAT I is predominately aluminum, only one structural damping coefficient γ is used. Usually, a viscous damping matrix C is present in Eq (1); however, there are no viscous dampers in PnPSAT I, damping is

purely a function of the complex modulus, $i\gamma$. The $\ddot{\bar{x}}(t) \in \mathbb{R}^{n \times 1}$ and $\bar{x}(t) \in \mathbb{R}^{n \times 1}$ represent the acceleration and displacement vectors, respectively *Doupe* [2009].

For the undamped free vibration case Eq. (3) can be written as

$$M \ddot{\bar{x}}(t) + K \bar{x}(t) = 0 \quad (4)$$

First, a synchronous solution is assumed of the form,

$$\bar{x}(t) = \bar{\phi} e^{i\omega t} \quad (5)$$

where ω is the radian frequency and $\bar{\phi}$ is a constant real-valued vector of dimension n . After substitution, a real-valued eigenvalue problem (EVP) is formulated

$$K\bar{\phi} = \lambda M\bar{\phi} \quad (6)$$

where the eigenvalue $\lambda = \omega^2$. Eq. (6) can be solved for the n eigenvectors $\bar{\phi}$ for n values of λ . However, typically only a few of the total number of eigenvectors and corresponding eigenvalues less than a predetermined cutoff are actually computed. Combining the m computed eigenvectors $\bar{\phi}$ into a matrix yields

$$U = [\bar{\phi}_1, \bar{\phi}_2, \dots, \bar{\phi}_m] \quad (7)$$

Both the mass and stiffness matrices are projected onto the eigenspace by

$$K' = U^T K U \quad (8)$$

$$M' = U^T M U \quad (9)$$

The now diagonalized mass and stiffness matrix allows for easier computation of the frequency response of the structure from an input force $F(\omega)$ from

$$X(i\omega) = U(-\omega^2 M' + (1 + i\gamma)K')^{-1} U^T F(\omega). \quad (10)$$

The magnitude $|X(i\omega)|$ and phase angle of $\angle X(i\omega)$ is computed from

$$|X(i\omega)| = \sqrt{[\text{Re}(X(i\omega))]^2 + [\text{Im}(X(i\omega))]^2} \quad (11)$$

$$\rho(\omega) = \tan^{-1} \frac{-\text{Im}(X(i\omega))}{\text{Re}(X(i\omega))} \quad (12)$$

where Re extracts the real values and Im extracts the imaginary values.

Plots of magnitude $|X(i\omega)|$ and phase $\angle X(i\omega)$ versus ω are useful tools in modal analysis. The peaks located in the magnitude plot indicate where the natural frequencies of the structure. Also, the modes can be extracted from the magnitude and phase information. In an optimization process, the eigenvalues and eigenvectors of the FEM model are tuned in order to match the experimentally measured natural frequencies and modes, respectively *Doupe* [2009].

2.4 Scanning Laser Vibrometer Data Collection Fundamentals

A few different methods can be used to acquire frequency response function (FRF) from a structure. The most common method involves the use of accelerometers. Accelerometers, as their name suggests, measures the acceleration of the subject being tested. Accelerometers are necessary in providing the data to create FRFs at each location of which have to be combined to create the overall mode shapes of the test subject.

Typically, dozens or more accelerometers are placed over a large test article. The addition of accelerometers can change the response of the system depending on the mass and stiffness of the test subject. However, in order to acquire an accurate representation of the mode shapes using accelerometers, hundreds of accelerometers may be required depending on the complexity of the

structure and accuracy required. This is why modern modal analysis is turning to the use of laser Doppler vibrometer (LDV).

LDV provides many different benefits, of which measuring test articles without contact provides the largest benefit. Also, it is possible to easily measure a tens to thousands of locations enabling a more accurate extraction of the modes, especially higher frequency modes.

The Polytech scanning laser vibrometer (PSV), model PSV-400-3d-M, is shown in Figure 6, and was used to collect data for modal analysis. The three laser heads are focused on the same point and utilize a Doppler effect method for measuring velocity. The Doppler effect is the change in frequency of a wave for an observer moving relative to the source of the wave. The most common example of this phenomenon is when a vehicle sounding its siren approaches. The siren will be higher pitched when traveling towards the observer and lower pitched as it travels away. Utilizing the Doppler equations, the vibrometer emits laser energy at a known frequency and measures the frequency of the reflected light to determine the velocity of the particular scan point on the test article *Doupe* [2009]. The Doppler equation, adopted from *Rees* [2001] is

$$\frac{\lambda_d}{\lambda_t} = \frac{\sqrt{1 - \frac{v^2}{c^2}}}{1 - \frac{v \cos \theta}{c}} \quad (13)$$

where c is the speed of light, v is the velocity of the scan point, θ is the angle of the detector in relation to the source, λ_t is the transmitted frequency, λ_d is the detected frequency.



Figure 6: 3 Head Scanning Laser Vibrometer

In the testing of PnPSAT I panels it was necessary only to use one laser head to measure the out-of-plane displacements. Measuring the in-plane displacements proved unnecessary because the in-plane modes have natural frequencies that far exceed the range of tuning conducted in this research. After complete alignment of the laser head, a grid of known coordinates from the FE model are loaded into the PSV software predetermining the measurement locations. Detailed information on the Polytec 3D LDV and PSV software can be found in *Polytec* [2007a] *Polytec* [2007c].

The acquired time domain data from the scanning laser vibrometer must first be converted to the frequency domain. The PSV software converts the time response data to the complex frequency domain through a fast Fourier transform (FFT). The continuous FFT is represented by

$$F(\omega) = \int_{-\infty}^{\infty} f(t)e^{-i\omega t} dt \quad (14)$$

where $F(\omega)$ is the frequency domain signal, $f(t)$ is the time domain signal, and ω is the frequency. However, since discrete sampling times are used to acquire the data the discrete Fourier transform (DFT) must be used. The DFT converts discrete time domain data into discrete frequency domain data. By

$$F_n = \sum_{k=0}^{N-1} f(t_k) e^{-int_k}, n = 0, \dots, N-1 \quad (15)$$

where N is the number of samples. In order to prevent aliasing, which occurs when two signals of different frequencies are sampled at such a rate as they are recorded as the same signal, an anti-aliasing filter is used. The PSV automatically sets the correct anti-alias filter once the desired frequency range is established by the user.

Leakage is another cause for error and is an effect of signals which are not periodic in the sampled data. It is caused by the finite of the data record, that introduce discontinuities across stop/start regions. In order to remedy leakage, a window is applied to the time response data. Various windows have been created for this purpose to include rectangular, Hanning, Kaiser-Bessel, flat top, and exponential. The windows of choice in impact testing are the force and exponential windows. The force window catches the quick impulse of the striking hammer. While the exponential window captures the output which is a large magnitude sinusoid initially because it was struck by the hammer then it ‘exponentially’ tapers off towards the end of the sample.

The complex frequency data is converted into an FRF. With the frequency domain data the vibrometer software calculates the FRF using

$$FRF = \frac{outputFFT}{inputFFT} \quad (16)$$

Unfortunately, this computation is more difficult than it appears. First the correlation functions must be determined using the general form

$$R_x(t) = \int_{-\infty}^{\infty} f(\tau)g(t+\tau)d\tau \quad (17)$$

from this the power spectral densities can be found by doing the FFT of the correlation functions.

The four power spectral densities with respect to the input $R(\omega)$ and the output $C(\omega)$ are

$$\begin{aligned} S_{CC}(\omega) &= C(\omega)\overline{C}(\omega) \\ S_{RR}(\omega) &= R(\omega)\overline{R}(\omega) \\ S_{CR}(\omega) &= C(\omega)\overline{R}(\omega) \\ S_{RC}(\omega) &= R(\omega)\overline{C}(\omega) \end{aligned} \quad (18)$$

were $R(\omega)$ and $C(\omega)$ are the FFTs of the input and output respectively. The over bar represents the complex conjugate. Given these power spectral densities, it is possible to get two FRFs, $H1$ and $H2$ given by

$$H1(\omega) = \frac{S_{CR}(\omega)}{S_{RR}(\omega)} \quad \text{and} \quad H2(\omega) = \frac{S_{CC}(\omega)}{S_{RC}(\omega)} \quad (19)$$

Both FRFs represent some form of output divided by input, but the $H1$ FRF is primarily affected by noise on the input. The $H2$ estimator is primarily affected by noise on the output. In general output noise is greater than input noise; hence, the $H1$ FRF is better for viewing. However, both FRFs should be almost identical when plotted so an averaging technique is used to minimize the noise. Each scan point is measured ten times; consequently each scan has four power spectral densities. Each power spectral density is averaged with the others of its same variable name then the averaged FRFs $H1$ and $H2$ are computed.

In order to ensure that the data is accurate, a test parameter, coherence, is used. Coherence is the ratio of $H1/H2$ and is a measure of consistency in the measured data. It relates how much of the output is directly caused by the input. Coherence ranges from zero to one, one being the input and output are perfectly related and zero being the input and output are totally unrelated.

After the scanning LDV has been setup correctly, it can be put in a scan mode where it takes ten measurements at each scan point until completion. The PSV software will classify the data based on valid, optimal, low signal, over range or invalidated. The over range data appears when the magnitude of the velocity is greater than the selected laser sensitivity. It is optimal to run the testing at night in order to minimize the effects of ambient noise. The scanning laser vibrometer and test article are very susceptible to noise to include anything from people walking near it or talking in the same room. Once completed the data is processed and used for tuning the FE model.

2.5 Finite Element Model Tuning

Costly and time consuming AIT testing can possibly be reduced or even avoided by the use of accurately tuned FE models. Tuning essentially means a model is corrected to accurately predict experimental data over a range of excitation frequencies. A tuned model should theoretically allow for the prediction of natural frequencies and modes of various configurations. Creating an FE model can vary significantly in difficulty. Regardless of complexity, creating an accurate model on the first attempt is hardly if ever realized. The process of tuning adjusts parameters in the FE model to more accurately predict responses to various loads. Tuning can be accomplished several different ways to include changing parameters which affect the mass, stiffness, or damping matrices. More commonly, the modulus of elasticity or material density; is

altered. In this research, only the modulus of elasticity's of the adapter ring and spring stiffness coefficients between the baseplate and -Z panel will be altered. A brief overview of FE model tuning is presented, next while the details can be found in Chapter III.

In order to accurately tune the FE model, experimental modal data of the test article first must be collected. To acquire the modes of the structure experimentally, the boundary conditions must be known. Boundary conditions typically support or constrain the structure. An example of a constrained structure is a satellite fixed on a shaker table to simulate the attachment to a rocket. In certain circumstances, it is better to allow the structure to float in order to keep the dynamic properties independent of any constraints or supports.

There are several devices used to excite a structure to include shaker tables, electromagnetic shakers, impact hammers, just to name a few. Modes whose natural frequencies are near the excitation frequency are excited. Once the structure is excited it is important to measure the input excitation and output response. As mentioned earlier, the output can be measured by accelerometers or laser vibrometers. Now an input-output relationship can be formulated in the frequency domain via FRFs where the peaks of the FRFs are the natural frequencies, as shown in Figure 7.

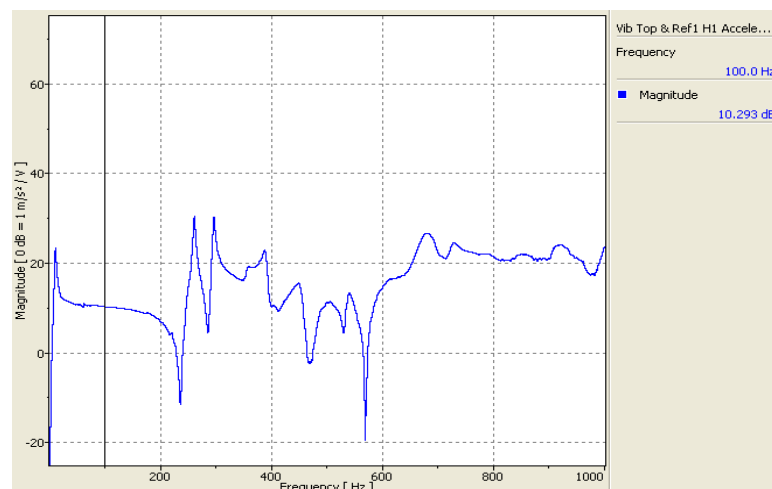


Figure 7: Frequency Response Function of -Z panel

Damping can also be calculated from the FRFs using the half-power bandwidth method. Taking measurements at multiple locations allows for the creation of operational deflection shape (ODS). Software utilizing a curve-fitting approach allows for the extraction of modes, damping factors, and natural frequencies from the FRFs and ODSs.

Upon extraction of the experimental data, tuning of the FE model can begin. The concept is to modify the eigenvectors to match the measured modes and the eigenvalues to match the square of the natural frequencies. In the tuning process, parameters affecting mass are not altered because the mass is an easily measurable quantity with a high degree of accuracy. Both of these parameters affect the stiffness matrix which in turn changes the eigenvectors and eigenvalues.

Due to the complexity and size of FE models it is nearly impossible to tune the FE model by hand. It is common to minimize an objective function which is a measure of the difference between measured and analytical responses. A common objective function is as previously presented and repeated here the difference between the measured and analytical eigenvalues and eigenvectors given as

$$J = \sum_{i=1}^p a_i \left[1 - \left| \frac{\lambda_i}{\bar{\lambda}_i} \right| \right]^2 + \sum_{i=1}^p \sum_{j=1}^r b_i \left[1 - \left| \frac{\bar{\phi}_{ij}}{\bar{\phi}_{ij} \hat{\phi}_{iN}} \right| \right]^2 \quad (1)$$

The weighting factors a_i and b_i can be adjusted to create a variety of objective functions for methods of comparison that place more importance on a particular mode or natural frequency.

λ_{iA} and λ_{iM} are the i^{th} analytical and measured natural frequencies, respectively, and $\bar{\phi}_{ijA}$ and $\bar{\phi}_{ijM}$ are the i^{th} analytical and measured eigenvectors or modes, respectively. The analytical eigenvectors are normalized with $\hat{\phi}_{ijN}$. The scalar summation limits p and r are the number of

desired modes and desired number of measurement locations, respectively. The absolute value operation on the last term is required because the overall sign of a particular eigenvector is unknown. The objective function J is minimized changing the parameters chosen while obeying the constraints in the FE model. By minimizing the objective function, the differences between analytical and measured natural frequencies and modes are reduced. This minimization approach can match natural frequencies quite easily, because they are simply scalar values, but it is much more difficult to minimize the differences between modes which are vector quantities. In the next chapter the details involving testing, modeling, and tuning will be presented.

III. Method

This chapter first describes the methods used to generate an untuned FE model for the $-Y$ and $-Z$ panels. Next, this chapter discusses how experimental data is collected to tune panel FE models. Finally, the PnPSAT I FE model is tuned and tested.

3.1 Method Overview

In order to create an FE model of PnPSAT I, only FE models of the $-Y$ and $-Z$ panels are created. Modal testing is conducted to collect modes and natural frequencies for both the $-Y$ and $-Z$ panels. The description of this testing will include the equipment used, test setup and theory. Also, the tuning process was applied to the $-Y$ and $-Z$ panels is described in detail. The tuned panel models are copied and attached to create a structure PnPSAT I FE model. Six DOF spring/damper elements keep the base plate and the adapter ring attached. The $-Z$ panel, base plate, and component point masses are connected via rigid links providing a fully developed PnPSAT I FE model. This FE model will be tuned once using this configuration to match KAFB experimentally collected data from the ORS office.

3.2 Generate $-Y$ and $-Z$ Panels FE Models

Modeling is seen as a way to reduce complex and expensive testing. Previous to this research effort a high order FE model was created by Spaceworks. High-order models are easily created from a detailed CAD file using automatic mesh generation feature found in most FE packages today. These auto-generated meshes generally possess many more nodes and elements than those that are carefully controlled by the analyst. Although generating a high-order model is initially less time consuming, the fact that the Spaceworks FE model has more than a million

DOF results in high demands on computing power to solve the eigenvalue problem. For example, approximately 18 minutes on 4 dual core AMD 8200 2.8G Hz processors with 64 gigabytes of RAM and requires 9.634 gigabytes of scratch disc space. On the same machine an eigenanalysis of the PnPSAT I can be completed in 3 minutes. The factor of six difference might not seem significant but during the optimization process, these eigenvalues and normal modes analysis is calculated hundreds to thousands, so of times this factor makes a significant impact. Also, during the optimization process, files are read and saved to disc because the matrices are too large to reside in RAM which dramatically slows down the tuning process because disc read write speed is dependent solely on the hard disc. Therefore, a reduced order FE model needs to be created for the tuning process to be computed in a reasonable amount of time.

The first step is to measure the mass of the $-Y$ and $-Z$ panels. When the FE model's mass is in close agreement with the measured mass then only the stiffness matrix has to be tuned. The $+X, -X, -Y, +Y$ panels are constructed in similar ways possessing the same properties to include structure, electronics, mass. The $-Z, +Z$ are constructed similarly. Hence, tuning the $-Y$ and $-Z$ panels is sufficient because once the two panels are tuned, they can be recopied and combined to create the outer structure of PnPSAT I. Addition of the components via rigid links allows for accurate tuning for the completed PnPSAT I. An overview of the process is in Figure 5, in Chapter I.

Each PnPSAT I panel is based on a clamshell design. The electronics are housed in the middle and the two outer panels are fastened together.

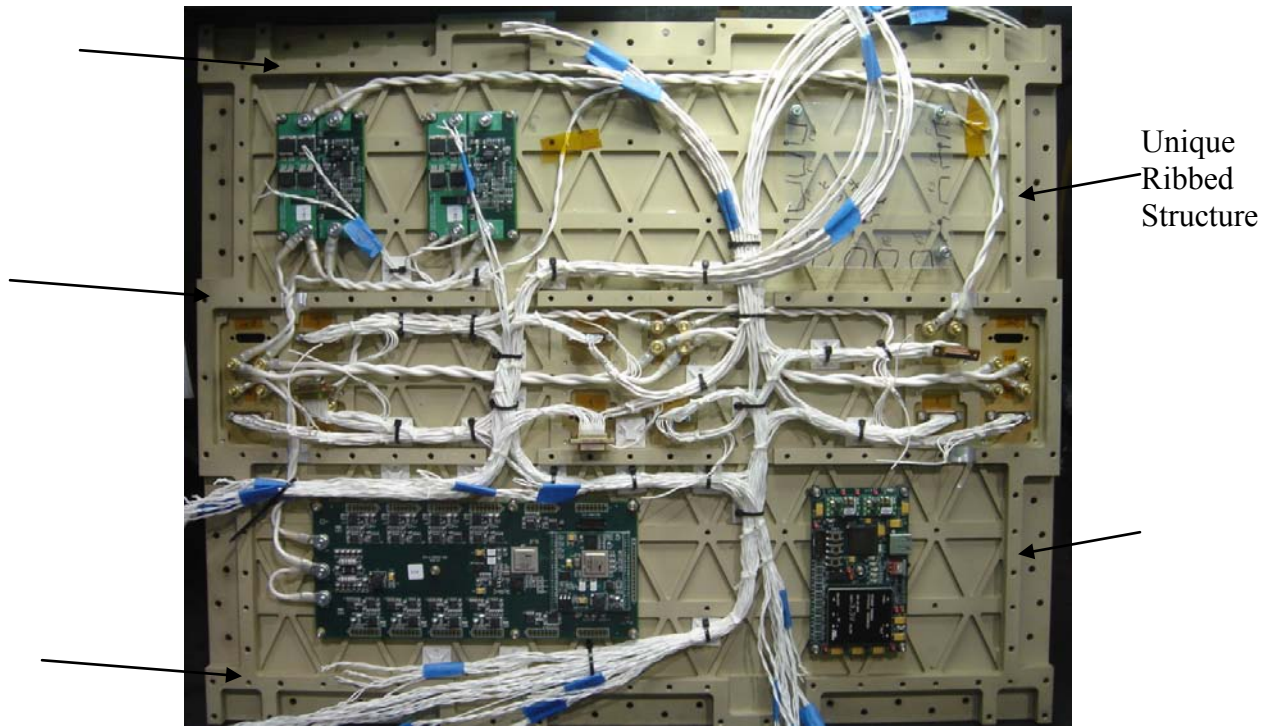


Figure 8: Picture of one half of PnPSAT I -Y panel with electrical components; arrows point out the unique ribbed structure which joins the two halves of the panel together.

Notice the ribbed interior and exterior of the panel. This design is unique in that it protects the electrical components and results in a very stiff but lightweight panel. Creation of the FE model of PnPSAT was initially generated from a detailed CAD file provided by Spaceworks. From the CAD model of -Y and -Z panels, reduced FE models were created. FEMAP, is a useful tool in creating and analyzing finite element models through a user friendly GUI (graphical user interface). The top shell of the -Z panel consists of geometry points, surfaces and solids shown in Figure 9.

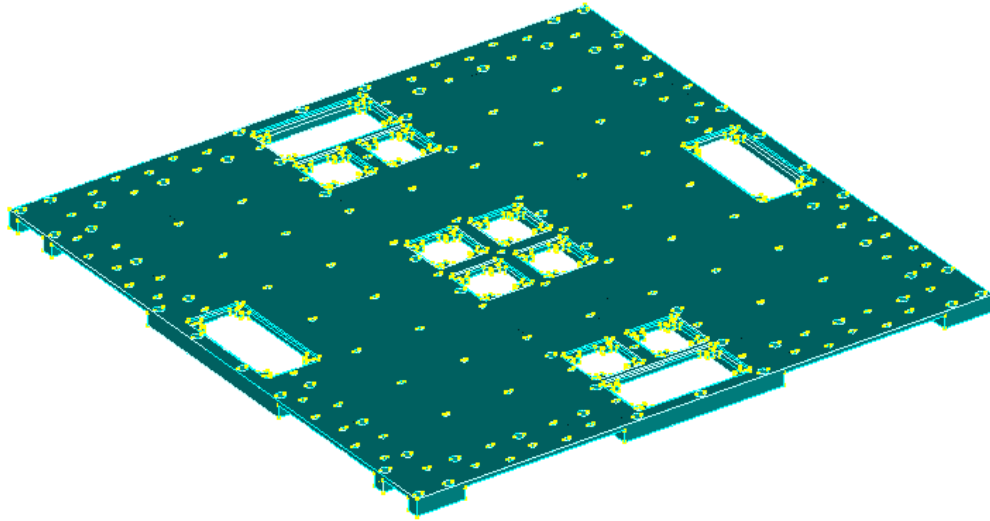


Figure 9: CAD geometry model of the -Z panel.

The next task consisted of creating a geometrically accurate FE model from the CAD files. Nodes are generated individually to ensure a continuous and accurate mesh. Starting with the corners and significant parts of the geometry the nodes are placed in a way as to ensure continuity and dynamics accuracy. Each node in Figure 10 was deliberately placed in order to ensure element's nodes would be coincident to each other. This ensures elements are rigidly attached and are not separating from one another.

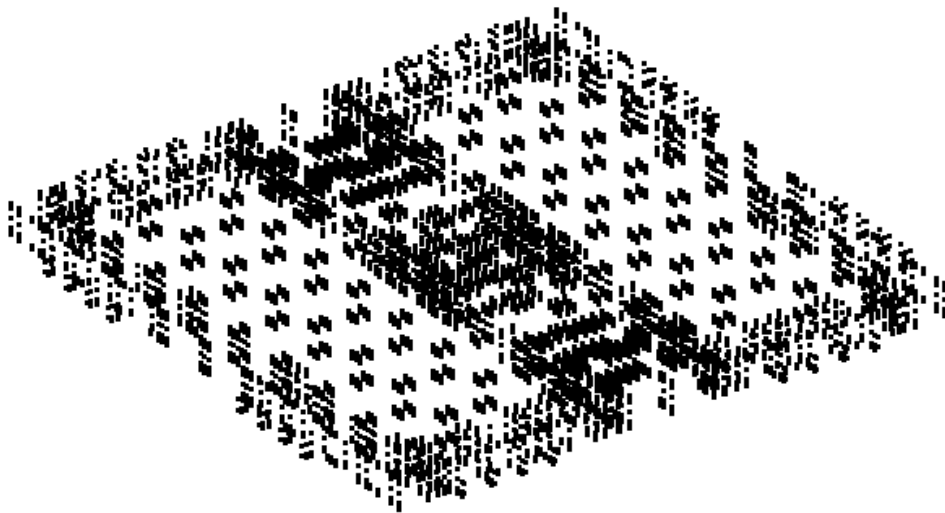


Figure 10: Nodal representation of the -Z panel.

Because the majority of PnPSAT I is modeled as 6061-T651 aluminum, each element is modeled with the same material properties; however, over 60 material property values are included in order to allow the tuning algorithm to adjust the stiffness properties of individual sections of the panel models. Therefore, the Young's moduli can be adjusted in the optimization process to correlate the FE model and the experimentally collected modes and natural frequencies.

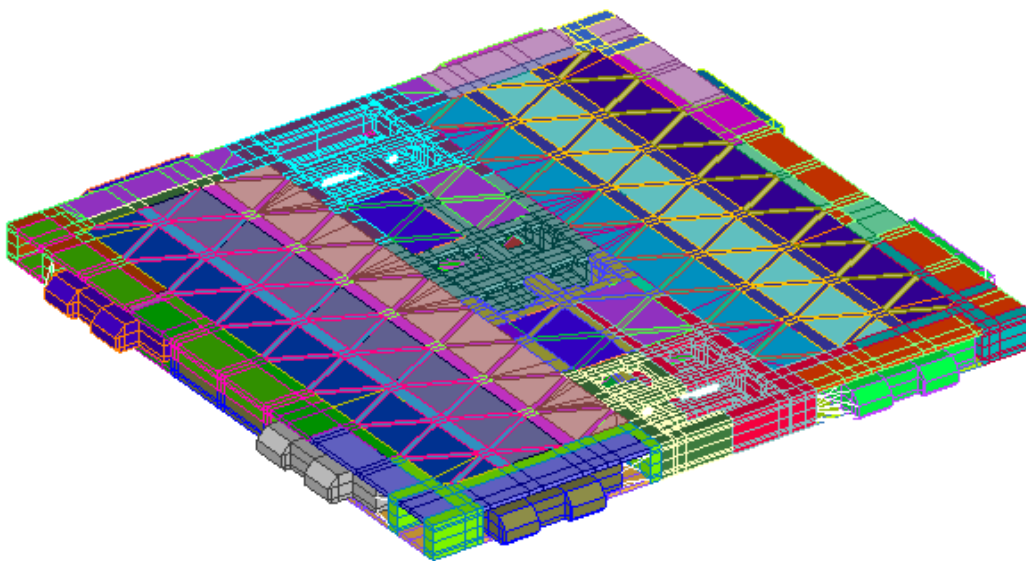


Figure 11: -Z Panel FE Model where, each color represents a different material card (95 total); these material card's properties are altered in the tuning process.

Approximately 89% of the elements are solid 8 node, 24 DOF hex elements. Each node of the hex solid element has 3 translational DOFs. It is easy to generate a FE mesh of solid elements from already created nodes. This generation is simply connecting the dots on a large scale. Approximately 10% of the elements are 3 node 18 DOF plate elements, which are used on the exterior structure of the panel. Ensuring the thickness of these plate elements agree closely with the actual satellite panel thickness was critical in matching the mass and more importantly, that the mode locations are in close agreement with the experimentally measured data. The

remaining elements were made up of rigid link elements which secured the hinges to the structure of the satellite.

A problem arose in the computation of the FE models mass matrix because the panel was not constrained. The MSC Nastran algorithm that creates the mass matrix produces a singular mass matrix when it shouldn't. This created havoc on calculation of the stiffness matrix and tuning process because it ruins the cross-orthogonality check (as is explained later). To remedy this, spring elements were inserted into the corners of the structure that have very low spring stiffness coefficients. These springs changed the first six rigid body modes to flexible modes with very small natural frequencies, six rigid body modes between 6 and 10 Hz. This alteration slightly changed the natural frequencies but left the mode shapes in the correct order.

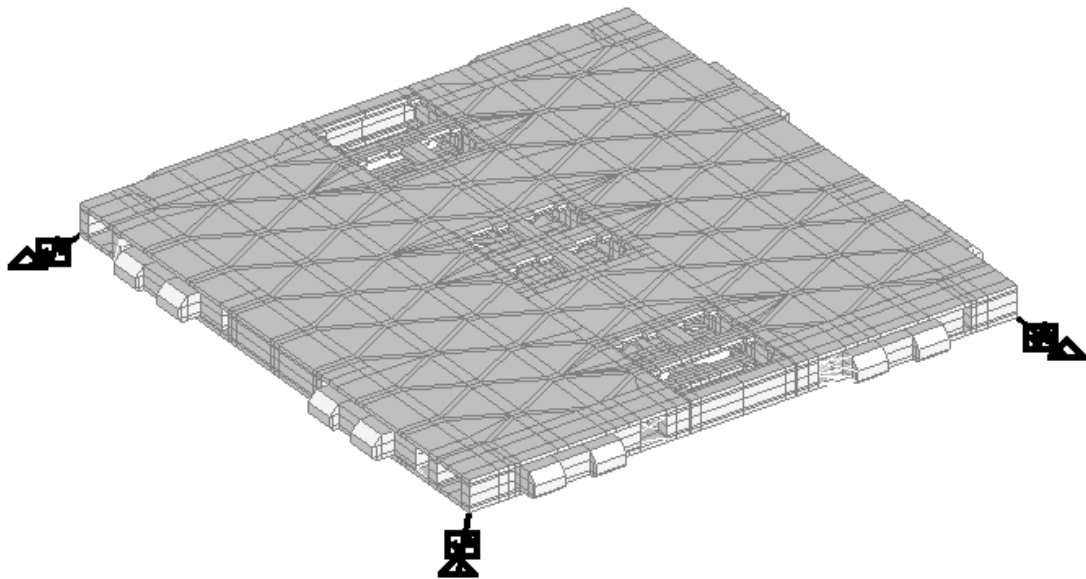


Figure 12: Transparent $-Z$ panel showing the spring dampers (black) in the corners with fixed node constraint. Elevates rigid body mode to avoid singular mass and stiffness matrices.

Both the $-Y$ and $-Z$ panels were constructed similarly and the next step is to tune the panel FE models but first the experimental data must be collected.

3.3 Test Setup

The PnPSAT I modal testing at AFIT consists of using a scanning LDV to collect velocity measurements over a grid of measurement locations on the surface of the satellite panels. PnPSAT I's panels are mechanically coarse structures which made choosing ideal measurement points difficult. An automated impact hammer is used to excite as many vibrational modes as possible in the spacecraft panels. The impulsive force imparted to the PnPSAT I panels is measured and used as the reference signal from which FRFs are computed from each measurement point, of which there are over 150 measurement points for each panel.

The test harness shown in Figure 13 is designed to simulate free vibration by minimizing the amount of strain in the panel boundary conditions. For true free-free boundary conditions, the panel ideally should be allowed to float freely in space. This is accomplished by suspending the panel by bungee cords. Two aluminum beams with pyramid shaped foam blocks on top, press on the bottom of the satellite providing light damping. The foam pads are necessary to damp out the system between strikes from the shaker. Elevating the foam pads provides increased damping. However, the pads are only adjusted to provide the minimal amount of damping to ensure the structure has stopped vibrating due to the excitation applied by the hammer.

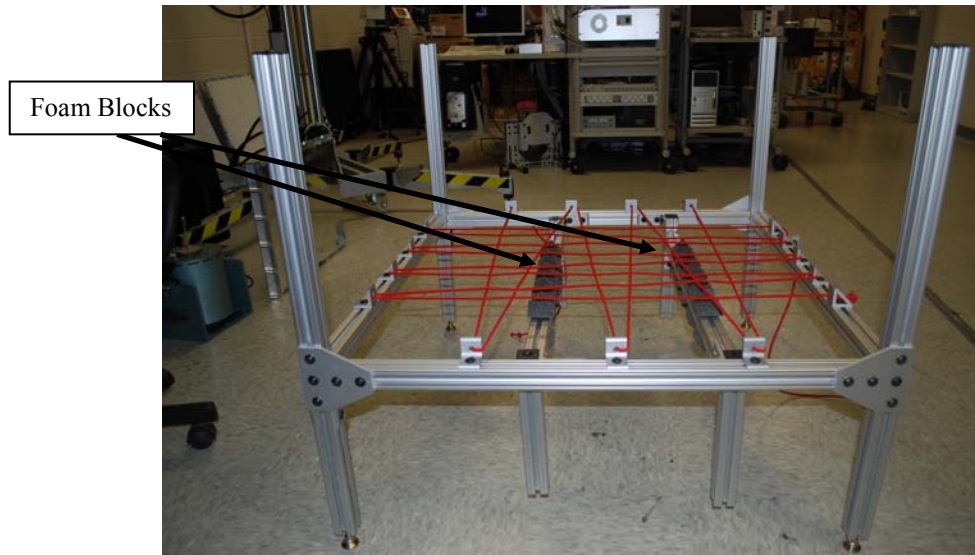


Figure 13: Test harness.

Once the test harness was setup, each panel was placed on the bungee cord and foam pads. A coating of a light scattering material is typically required as a surface treatment when collecting LDV data; however, due to PnPSAT being flight hardware with onboard electronics, applying a coating on the panels was not an option. Next, a reference coordinate frame for the scanning LDV is defined. From the FE model, approximately 150 nodes are selected at which measurements are taken. The selected nodes are all on the same plane and are located at least 1cm from the edge or any screw holes to ensure that the laser head can take unobstructed measurements. The next step is a careful 2D alignment of the laser. The 3D coordinates of each selected node are imported into the PSV software. Only one of the three laser heads are used because the velocities are only measured out-of-plane making the other two vibrometer heads unnecessary. In order to teach the laser vibrometer the test article coordinate system, several points of known coordinates are required. To achieve the highest accuracy of these locating points, precision calipers were used to measure the surface location of four nodes near the corners of the panels. Reflective tape and a pen point are used to mark the location of these four nodes as indicated by the circles drawn in Figure 14.

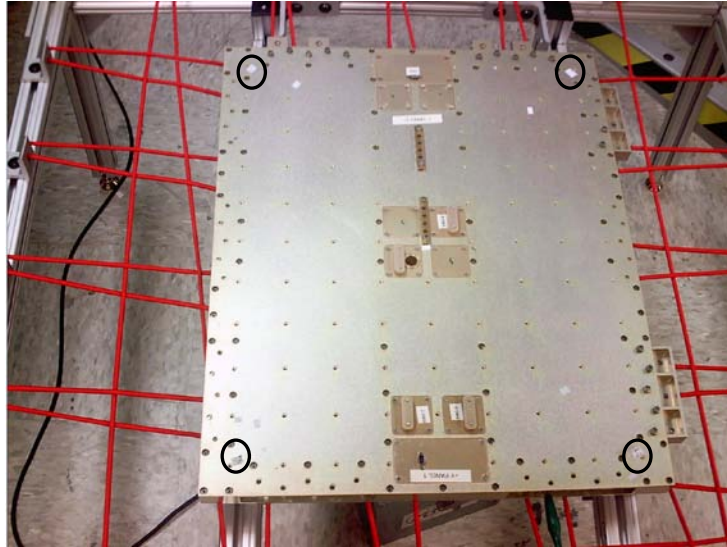


Figure 14: PnPSAT -Y panel with precise nodes and arbitrary points, reflective tape located on corners.

An electromagnetic shaker set to act as an automatic ping hammer (Figure 15) provides impulse like excitations. A Hewlett Packard 33120A 15MHz/Arbitrary waveform generator is programmed to generate a narrow pulse given a specific amplitude and frequency width.

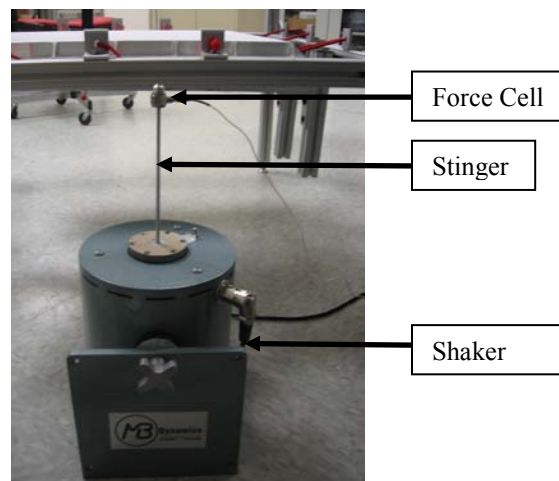


Figure 15: MB Dynamics Cal50 exciter electrodynamic shaker, setup to perform as an automatic ping hammer.

These impulsive single strike impacts are set to occur every ten seconds to allow for the system to damp out before striking again and theoretically excite all frequencies. However, most

of the energy is shown in the lower frequencies. Impact excitation was chosen for this research primarily because the excitation device is not attached to the test article which would change the response of the structure. Impact excitation also provides much better coherence than other methods. As previously described, coherence is the measure of the linear correlation between input and output or how much the response of a structure depends directly on the excitation input. A display of the coherence during the test of the $-Z$ panel is in Figure 16.

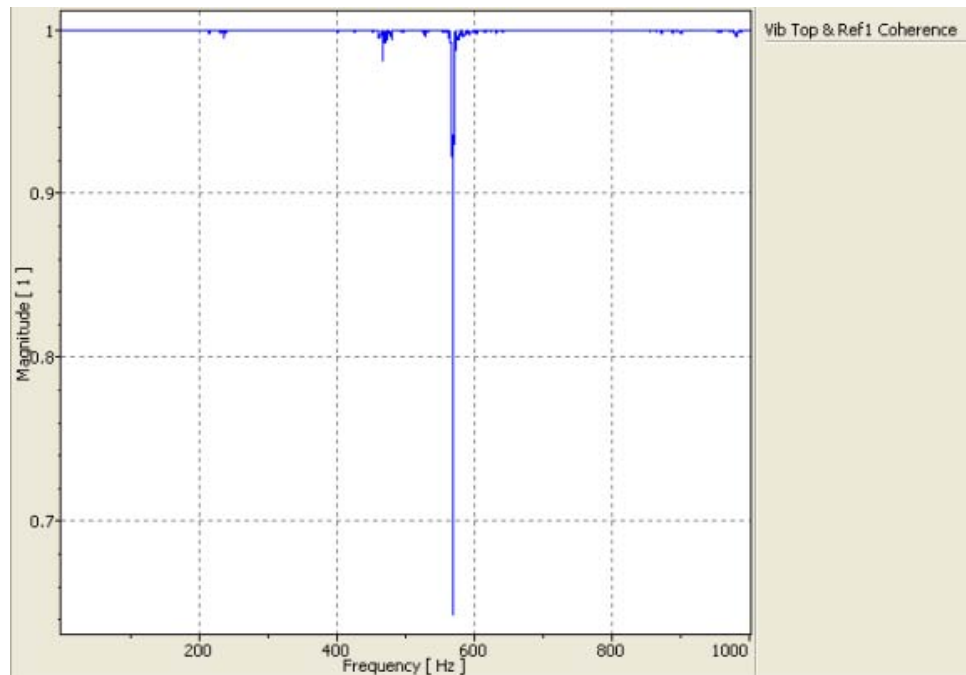


Figure 16: Coherence of testing on the $-Z$ panel.

A threaded rod, called the stinger, connects the shakers actuator to a force cell which has a flat plate at the other end (Figure 15). Transducers inside the force cell vary an applied voltage corresponding to the impact force magnitude. The force cell data is sent through a signal conditioner, which amplifies the signal, and then to the vibrometer as a reference input.

The shaker is placed underneath the test stand oriented so that it strikes the panel at a desired excitation location as shown in Figure 17. Multiple strike locations are necessary to ensure that

all the modes are excited; if the shaker strikes the panel at a modes' nodal line that mode will not be seen in the measured deflection shapes.

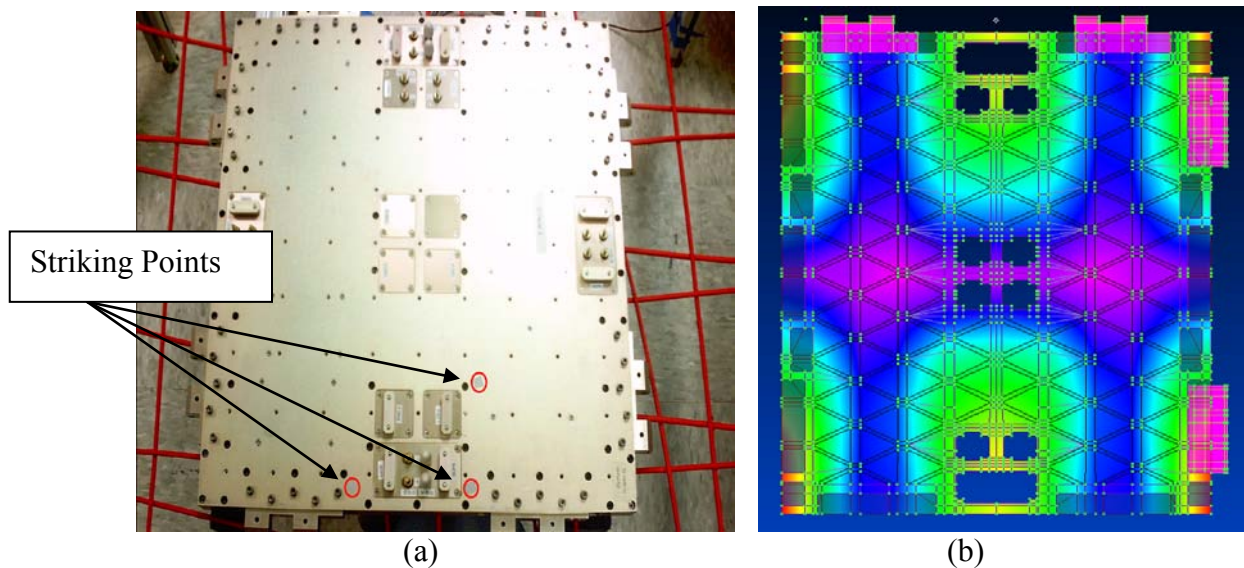


Figure 17: (a) Shaker striking points on bottom side of panel (tested facing other direction) (b) picture of the fifth mode, dark regions represent nodal lines.

An important parameter to monitor on the input excitation signal is spectral density. This is the amount of power imparted to the structure at each frequency. *Friswell and Mottershead* [1995] provides a good discussion on spectral density (aka power spectrum). A typical spectral density plot is shown in Figure 18. A general rule of thumb is to keep the spectral density within 10 dB to 20 dB of the starting value throughout the frequency of interest. If the spectral density drops off too quickly, sufficient energy will not be imparted into the structure at higher frequencies resulting in poor measurements at these frequencies. Spectral density can be affected by hardness of the impact plate connected to the force cell, magnitude and duration of the impulse from the shaker, and mass ratio of test article.

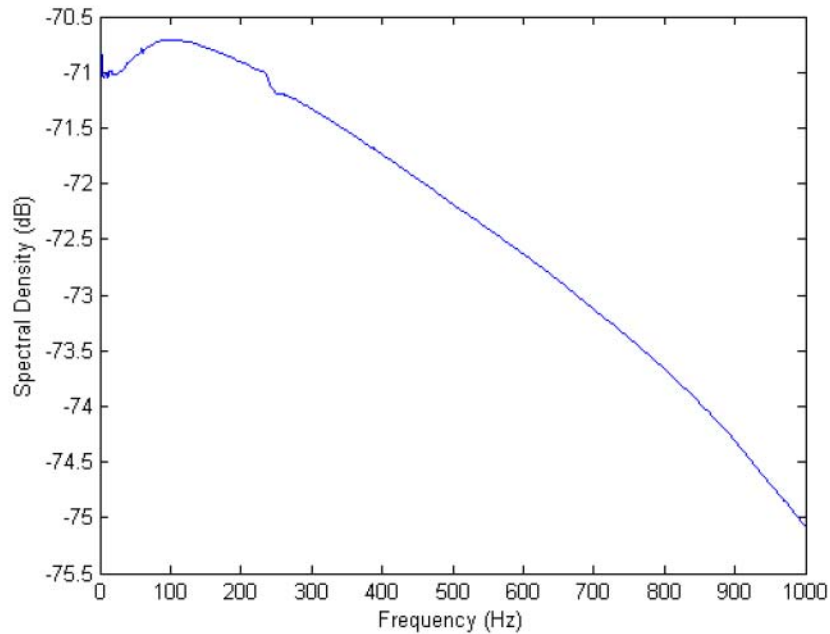


Figure 18: Spectral density plot of an impact excitation *Doupe* [2009].

Yet another important characteristic to monitor during impact excitation is the time domain signal of the input. The time domain signal should look as close to a theoretical impulse as possible. However, in reality, the force cell will output small changes in voltage at the beginning and end of an impulse strike as the striker begins to accelerate and again as it returns to its original position after the strike. These changes appear as side lobes to the main impulse in the time domain and must be minimized to ensure a clean strike. The anomalies can be minimized by adjusting the magnitude and frequency settings of the waveform generator. Large side lobes on the time domain input have an adverse affect on coherence and reduce the quality of the data collected. Adjustments attempting to eliminate side lobes can also lead to the striker hitting the panel multiple times during one impulse because the impulse width is too large.

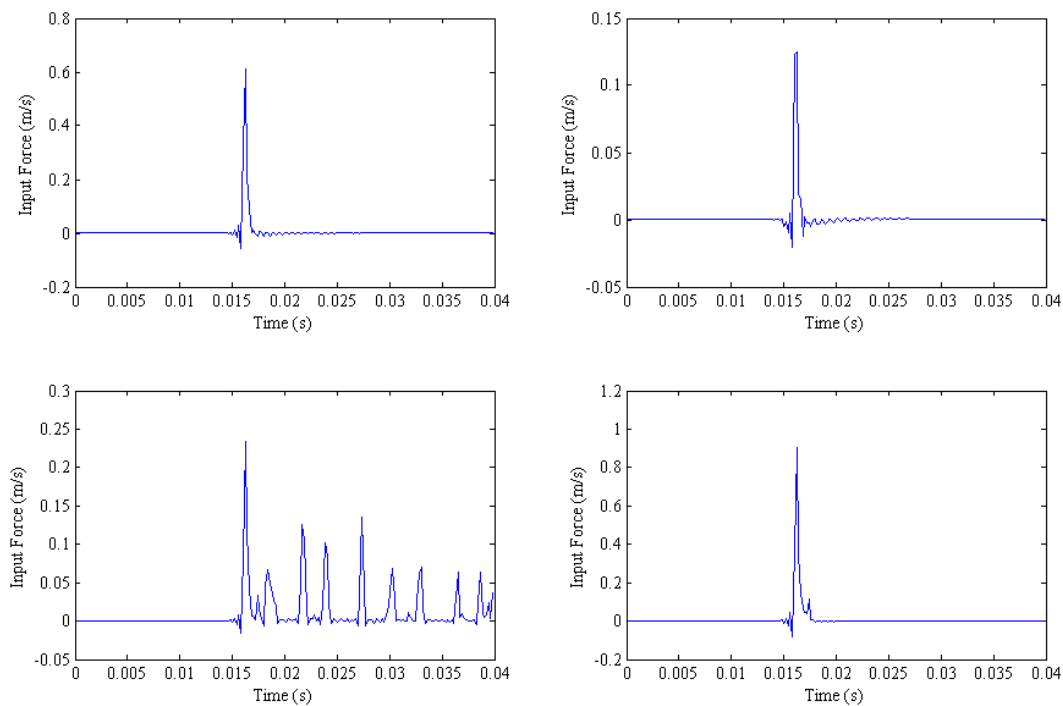


Figure 19: Top Left: A good impact excitation. Top Right: A squared-off peak on pulse indicates that the hammer struck the test article too slowly. An adjustment of the pulse width is necessary. Bottom Left: The striker hits the panel multiple times indicating both frequency and magnitude needs to be adjusted. Bottom Right: Side lobes indicate that the magnitude is too high *Doupe*. [2009]

The panel's dynamic response is collected over a range of frequencies from 0-1000 Hz. Figure 20 plots the grid of measurement locations that were selected in the FEM model and exported to the PSV software for each panel. The top laser head of the vibrometer focuses on each point in succession and records the velocity as a function of time as the panel is excited.

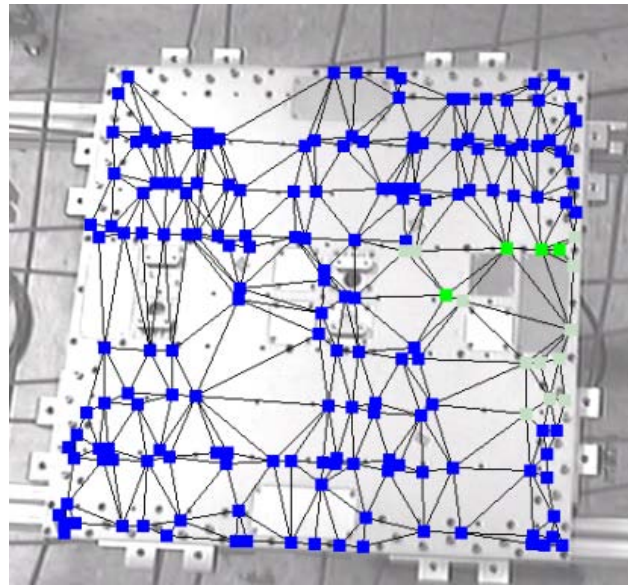


Figure 20: Typical node points on the -Z panel from PSV. Points picked from FE model to avoid holes and scratches. Blue means unmeasured, green means successful measurement and gray means over ranging typically caused due to people talking or walking around the room.

The excitation force for each impact is recorded as a function of time as well. Each impact of the ping hammer triggers the vibrometer to collect data for the programmed period of time (10 seconds) and with the programmed sampling rate. The sampling rate must be 2x greater than the signal to avoid aliasing. The default setting in the PSV software for the sampling rate is 2.56 times the maximum frequency of interest to avoid aliasing.

The test setup is extremely sensitive in that it cannot be touched once aligned and calibrated. The LDV can collect very small motions, for example, talking and closing doors are easily detected see Figure 20. Due to sensitivity to noise, tests were conducted at night to avoid any erroneous measurements. Testing at night ensured more accurate results and avoided over

ranging of the lasers. Each point was measured ten times and averaged in the frequency domain to minimize noise effects. A picture of the complete test setup using the -Y panel shown in Figure 21(a).

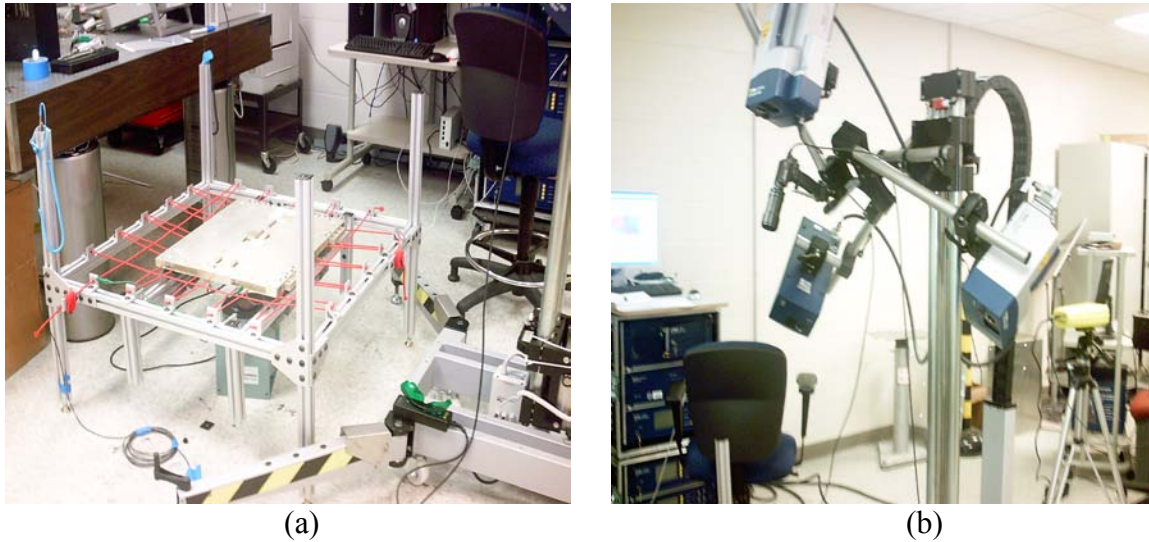


Figure 21 (a) Satellite panel in test stand and (b) PSV-400-3D LDV.

3.4 Mode Shape Extraction

The PSV software computes a FFT of the time response data for each DOF at every valid measurement location. The user can select to animate the operational deflection shapes (ODS), in the time domain. An ODS is representative of the actual displacement of the panel at a specified frequency. Therefore, all the modes are present in some form in an ODS with the exception of modes that are not excited. The ODS is dependent of the input location and magnitude of the force applied. Any changes to either input location or magnitude the ODS will likely change. For example, if the test article is unconstrained and it is struck with too much force near the outer edge of the panel, a rigid body mode will appear dominant. Each ODS contains many modes but is typically dominated by a single mode, when the user is selecting a

frequency near resonance. The mode shapes are extracted from the measured ODSs using the modal extraction software ME-Scope VES 5.0.

ME-scope imports FRF data directly from the PSV software through a proprietary Vibrant Technologies file format. ME-Scope's software utilizes curve fitting algorithms to generate an FRF. A transfer function is calculated by assigning poles and zeros to the FRF corner frequencies. The calculated transfer function fits a similar curve to the measured FRF. Natural frequencies, damping, and mode shapes are then estimated from the transfer function. The modes are independent of the loads imparted on the structure during the test. ME-scope can also animate the modes by scaling the eigenvectors with a sinusoidal magnitude function in the time domain. Animating these different modes allows for a visualization of each particular node and erroneous data can easily be discovered and eliminated. Typically, these bad data points arrive from scattering of the laser light resulting in a poor return to the LDV sensor. As mentioned earlier, a light scattering material which is typically used when scanning metallic surfaces wasn't used because PnPSAT is flight hardware. This led to the laser hitting scratches in the metallic surface leading to some erroneous data; needless to say, all 3 DOF for each bad data point was dismissed. Due to the scattering effect, 30% and 18% of the data points for the $-Z$ and $-Y$ panels, respectively, were removed. After eliminating bad data points and extracting the complex-valued modes, the next step is to analyze the data.

Before the extracted mode shapes can be utilized for FE model tuning, the extracted complex-valued mode shape matrix $\bar{\Phi}_C$ is approximated to a real-valued mode matrix $\bar{\Phi}_R$ by *Neidbal's* [1984] complex transformation:

$$\bar{\Phi}_R = \text{Re}(\bar{\Phi}_C) + \text{Im}(\bar{\Phi}_C) \left[\text{Re}(\bar{\Phi}_C)^T \text{Re}(\bar{\Phi}_C) \right]^{-1} \text{Re}(\bar{\Phi}_C)^T \text{Im}(\bar{\Phi}_C) \quad (20)$$

where all values are defined in Nomenclature. Based on previous research efforts, *Doupe et al* [2009], it was found Neidbal's complex transformation yielded the best results for this case.

3.5 Tuning -Y and -Z panels

After converting the complex-valued modes to real-valued, the tuning process can begin. The optimization process will adjust various stiffness related parameters in the FE model until the natural frequencies are tuned to be within a predetermined tolerance and the difference between the measured and analytical modes is minimized. Again, the objective function that is minimized is,

$$J = \sum_{i=1}^p a_i \left[1 - \left| \frac{\lambda_i}{\bar{\lambda}_i} \right| \right]^2 + \sum_{i=1}^p \sum_{j=1}^r b_i \left[1 - \left| \frac{\bar{\phi}_{ij}}{\bar{\phi}_{ij} \hat{\phi}_{iN}} \right| \right]^2 \quad (1)$$

at each optimization step the eigenvalues and modes are compared to the measured. For tuning the panels $a_i = 0$ and $b_i = 1$; meaning the objective function minimizes the difference between the modes while constraining the natural frequencies separately with a tolerance given by the analyst. Nastran uses a gradient-based optimization method in order to minimize the objective function. A gradient-based approach calculates partial derivatives of the objective function and minimizes the objective function in a few steps as possible by adjusting the previously mentioned model parameters in the direction of steepest descent.

The first step is to generate the mass matrix which remains constant throughout the tuning process. In order to calculate the reduced mass matrix a Guyan reduction is completed. The Guyan reduction simply takes the measured DOFs, which are the basis for the tuning process, and extracts them from the FE model. The Guyan reduction is described by:

$$\begin{bmatrix} K_{11} & K_{12} \\ K_{21} & K_{22} \end{bmatrix} \begin{bmatrix} x_1 \\ x_2 \end{bmatrix} = \begin{bmatrix} F_1 \\ F_2 \end{bmatrix} \quad (21)$$

where K is the stiffness, x_1 are the measured DOF and x_2 are all other DOF. F is the applied load and for this case it is zero. From this, solve the linear system of equations to arrive at

$$x_2 = -K_{22}^{-1} K_{21} x_1. \quad (22)$$

The Guyan reduction matrix is:

$$G = \begin{bmatrix} -K_{22}^{-1} K_{21} \\ I \end{bmatrix} \quad (23)$$

where I is the identity matrix. The Guyan reduction matrix can be applied to the mass matrix.

$$M_{AA} = G^T M G \quad (24)$$

This operation will reduce the mass matrix to the size of the measured DOFs. This matrix is important for the cross-orthogonality check.

In order to ensure convergence and a reasonable solution, constraints are put on the parameter. Typically Young's moduli are allowed to vary up to +/- 20% of the initial table values. The natural frequencies have a fixed constraint of +/- 5% from the measured.

Mode tracking is also used in order to ensure that the modes remain in the initial order. Mode tracking is done with a cross-orthogonality check between the mass normalized eigenvectors from the current and previous optimization steps and the mass matrix, represented by the equation below:

$$\Phi_i^T M_i \Phi_{i-1} = t_i \quad (25)$$

where i is the current design cycle and t_i is a n by n matrix. If the eigenvectors do not change between optimization cycles, the t_i will be the identity matrix. If the eigenvectors change between optimization cycles, some of the values on the diagonal will be less than 1.0. If the mode order has changed indicated by any diagonal value falling below 0.9 Nastran then corrects the mode order even though the associated natural frequencies will be out of order. This mode tracking function is important because the optimizer must correctly match eigenvectors with the target modes.

3.6 Creating Entire PnPSAT I Using -Y and -Z panel

After tuning the -Y and -Z panels, the complete PnPSAT I model can be assembled. In FEMAP, both the -Y and -Z panels are imported into a single FE model and joined together. The panels are connected with blocks; a view of two of PnPSAT I panels open and connected is in Figure 22.

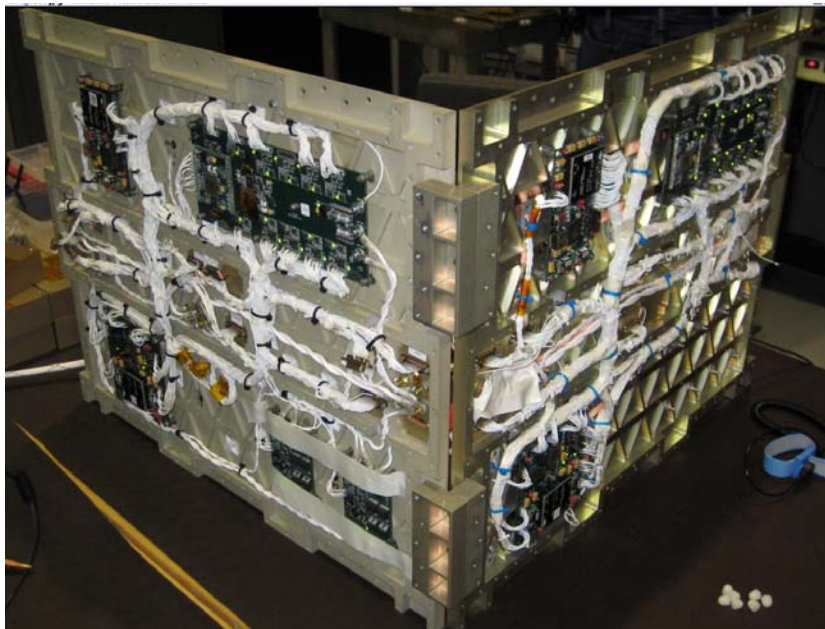


Figure 22: PnPSAT I panels open and joined together via hinges.

Because the +Y, +X, -X panels are identical to the -Y panel, the tuned -Y panel FE model can be copied to create -Y, +X, -X panel FE models. The +Z is identical the -Z panel, the tuned -Z panel FE model can be copied to create the -Z panel FE model. Two components influential on the tuning process of PnPSAT I were the base plate and SPA adapter ring. The base plate was acquired from the high-fidelity Spaceworks model, Figure 23(b), and the adapter ring, Figure 23(a), was created from 3 adjacent plate elements. The bottom of the adapter ring is constrained in all degrees of freedom.

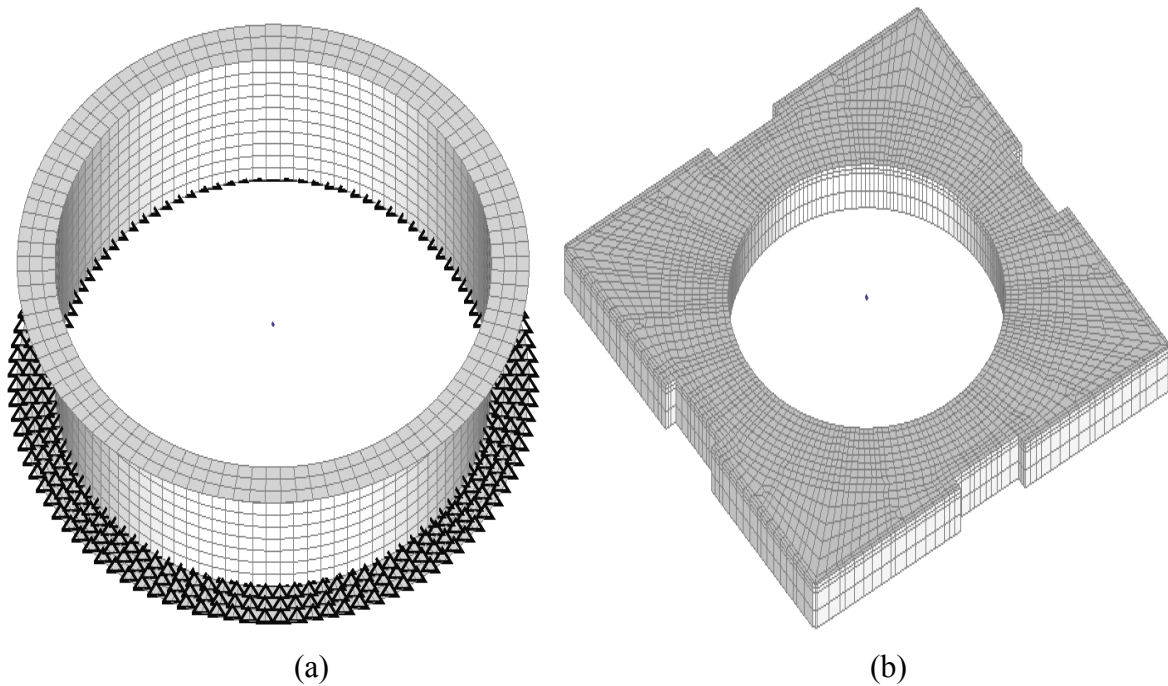


Figure 23: (a) Adapter ring modeled with plate elements, constraint forces attached (b) base plate acquired from Spaceworks model.

Initially, the panels were to be connected using spring elements; however, when the panels were joined together the nodes on the side panels became coincident; meaning nodes from each panel became a single node sharing elements from both panels. A coincident node check of the entire satellite merged the nodes fundamentally rigidly attaching the panels together. The coincident nodes can be visualized in Figure 24(a). The SPA adapter ring has constraint forces

on it. These constraint forces constrain the three translational and three rotational, making each node constrained in all six DOFs. The constrained adapter ring is attached via spring damper elements to the base plate (Figure 24(c)). These spring damper elements' stiffness parameters will be tuned to ensure the FE model is as close to the experimental natural frequencies as possible.

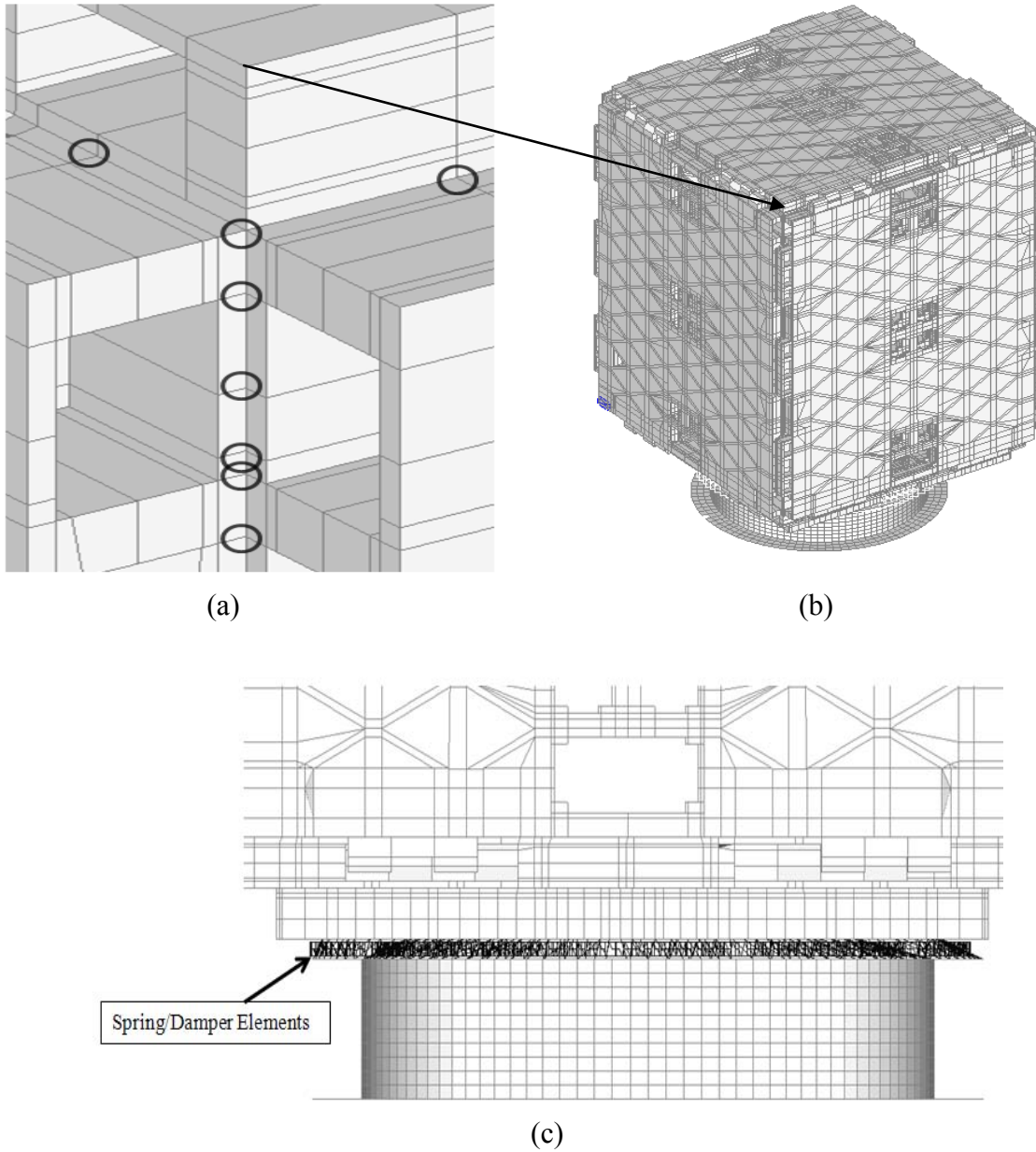


Figure 24: (a) Demonstration of coincident nodes (b) constructed PnPSAT I (c) side view of the spring elements connecting the adapter ring to the base plate.

The base plate is rigidly attached to the bottom of $-Z$ panel. The constructed satellite structure can be seen in Figure 24(b). The components of the satellite to include antennas, GPS receivers, solar panels, batteries are modeled as single point mass elements. The components are defined by their mass and the principle MOI which came directly from the Spaceworks FE model. A quick check to make the sure the components are the correct mass and in the right place is check total mass and center of gravity (C.G.). Each element is rigidly linked to nodes near it, in essence providing an accurate yet more simplified model. A look into the satellite at the components on the interior is provided in Figure 25.

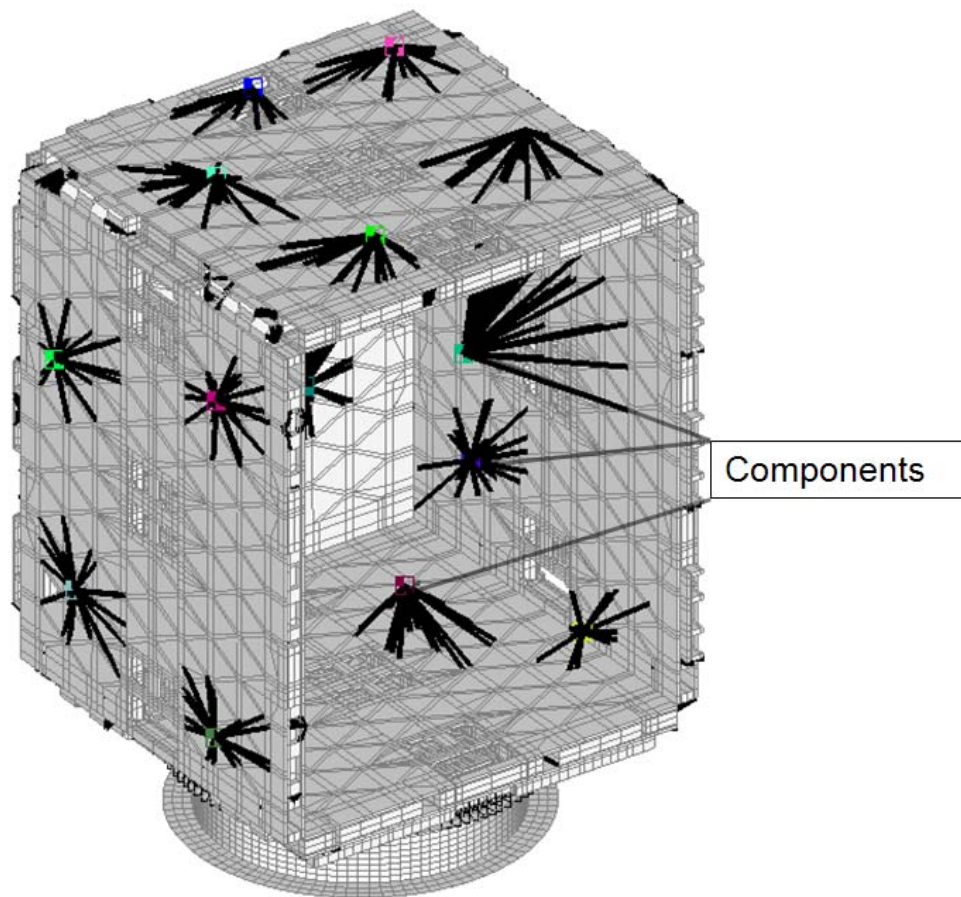


Figure 25: Look into PnPSAT I FE model showing interior components attached via rigid links.

The complete PnPSAT I FE model is in Figure 26.

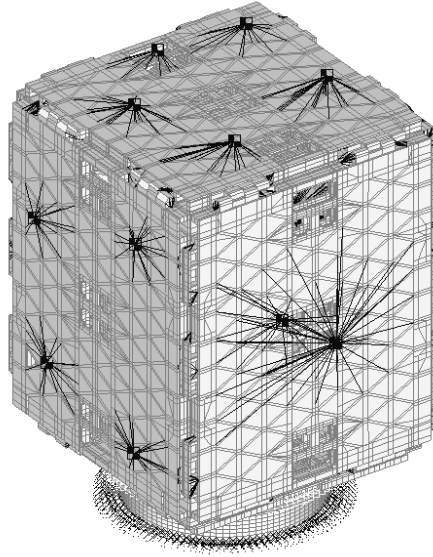


Figure 26: Complete PnPSAT I model with components connected by rigid links.

3.7 Measurement Method for Frequency data for Entire PnPSAT I

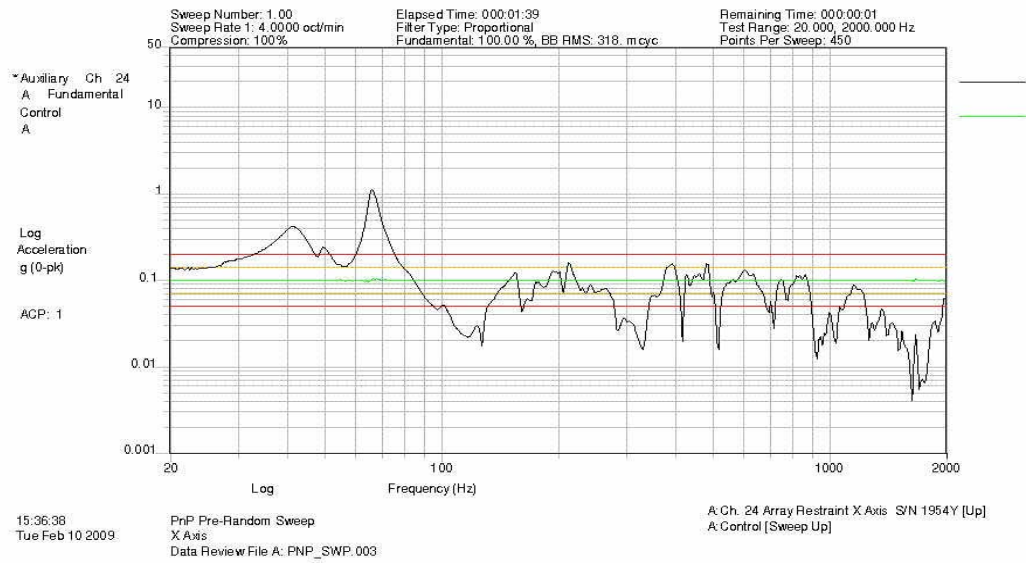
Now that both the panels are correctly tuned and the untuned full scale model is created the next step is to tune the entire satellite. The method used to conduct the forced response testing or vibration of the entire satellite was conducted at Kirtland AFB in Albuquerque, New Mexico. A shaker table, as shown in Figure 27, applied a burst random vibration and burst sine ranging from 0 to 2000 Hz. This shaker table is considered electro hydraulic; with hydraulic shakers, force is generated through the use of hydraulics, which can provide much higher force levels than other shakers. The best choice of excitation function depends on several factors such as the available signal processing equipment, characteristics of the structure, general measurement considerations and, of course, the excitation system. In this case, burst random vibration and burst sine vibration were chosen. However, other various excitation functions and methods exist and possibly better exploited given the differences in factors mentioned above.

Now that the methods for testing have been described, the method for acquiring the data for this experiment must be explained. In this case, accelerometers were placed on the satellite in several different places. These are noticeable in Figure 27 represented by the wires coming off the satellite hanging down from the shaker table.

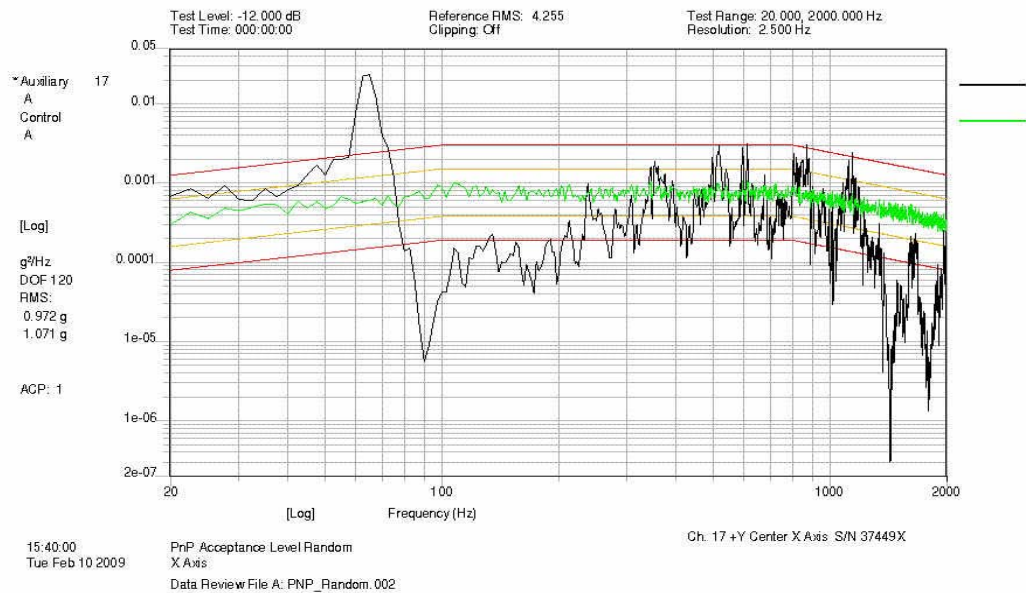


Figure 27: PnPSAT I on the vibration table on Kirtland AFB.

The satellite is tested in all three axes. Each accelerometer is aligned with each axis. With this data and using the process described in Section 2.4, the FRFs of each different axis case can be computed. Examining the FRF it is easy to estimate natural frequencies. The first few natural frequencies from the three different tests are used for tuning. However, the mode shapes of PnPSAT I were not taken and therefore the untuned model will necessarily be representing the correct mode shapes as the actual satellite would behave. An example of the accelerometer data taken during the test of the X axis test is given in Figure 28; also, a comparison between the X axis random vibration sweep and sine sweep FRF.



(a)



(b)

Figure 28: (a) FRF of Sine sweep from 0 to 2000 Hz on X Axis test (b) FRF of random vibration sweep from 0 to 2000 Hz on X Axis Test, green represents input and black represents output.

3.8 Tuning PnPSAT I

PnPSAT I's tuning process involved minimizing difference between the first three KAFB measured natural frequencies and the FE model natural frequencies to within +/- 5%. The modal data was not extracted from the KAFB data due to the limited number of accelerometers, so mode tracking is not required; because the panel stiffness and mass properties were previously tuned as explained earlier in this document. The -X, +X, -Y, +Y, -Z, Z panel's material cards remain constant throughout the tuning process. The 6 DOF spring/damper element's stiffness and the base plate and adapter ring's Young's moduli serve as the tuning parameters. There are a total of 148 spring/damper elements in Eq. (19) in the model that can be tuned, where $a_i = 1$ and $b_i = 0$. Attached are 18 property cards; each property card possesses 6 DOF allowing for 108 design variables. An additional 20 design variables are the adapter ring and base plate Young's moduli, totaling 128 design variables. The design variables are altered by Nastran in a gradient-based optimization approach in order to minimize the objective function. Convergence is achieved when the objective function cannot be minimized further by manipulation of the design variables. Constraints are applied on the 6 DOF spring coefficients by allowing the spring/damper elements to be altered by .01% to 1000% of their original values. The Young's moduli are constrained to be within +/-40% of their original table values. In the next chapter we discuss the results.

IV. Results and Discussion

In this chapter the tuning results of the $-Y$ panel and $-Z$ panel, and satellite FE model are presented. In each section, the untuned FE models are presented followed by a comparison of the tuned model to the experimental data.

4.1 Untuned $-Y$ and $-Z$ panel FE model Results

First, we look at the untuned panel FE model modes and natural frequencies to ensure the experimental and FE models modes agree with respect to each other. In order to assume the mass matrix is correct the mass of the FE model must match to within a 1%. It is important that the FE model is in close agreement with measured mass. The difference between the measured and model masses should be within 1%. A comparison between measured and analytical is summarized in Table 1.

Table 1: Comparison between actual and model mass.

	Measured (kg)	Analytical (kg)	% Difference
-Z Panel	6.72	6.7077	0.183035714
-Y Panel	6.82	6.8589	0.570381232

The untuned $-Y$ and $-Z$ panels have fewer FE DOF than the Spaceworks FE panel models. The comparison between the number of nodes and elements for each panel is summarized below.

Table 2: Comparison between Spaceworks and newly created untuned $-Y$ and $-Z$ FE models.

	Spaceworks -Z Panel	Spaceworks -Y Panel	Reduced -Z Panel	Reduced -Y panel
Nodes	~42,000	~48,000	7,647	8,875
Elements	~28,000	~30,000	4,445	5,273

It is important to ensure no mechanisms or localized modes exist in the untuned FE models. An eigenvalue and normal mode shape test is run on the untuned models. This test gives the

natural frequencies along with the corresponding modes. Looking through the mode shapes calculated it is important to ensure that the experimental and analytical modes agree in order for the tuning process. Upon inspection of these modes it was evident that local modes existed. These local modes were caused by elements not being properly linked to each other, typically the rigid link elements which connect the hinges on each panel. To fix this problem all the rigid links in the model were erased. The second time around it was critically important to make the hinge node be dependent, while making the panel itself the independent nodes. This ensured that whatever the nodes on the panel were doing the dependent nodes would mirror. Successfully eliminating this localized mode problem thereby allowing for the modes to line up. The six mode shapes for both panels will be compared to the six measured mode shapes. Refer to Figure 29 for the -Y panel and Figure 30 for the -Z panel; note, the measured mode shapes are interpolated from the points measured by the scanning LDV.

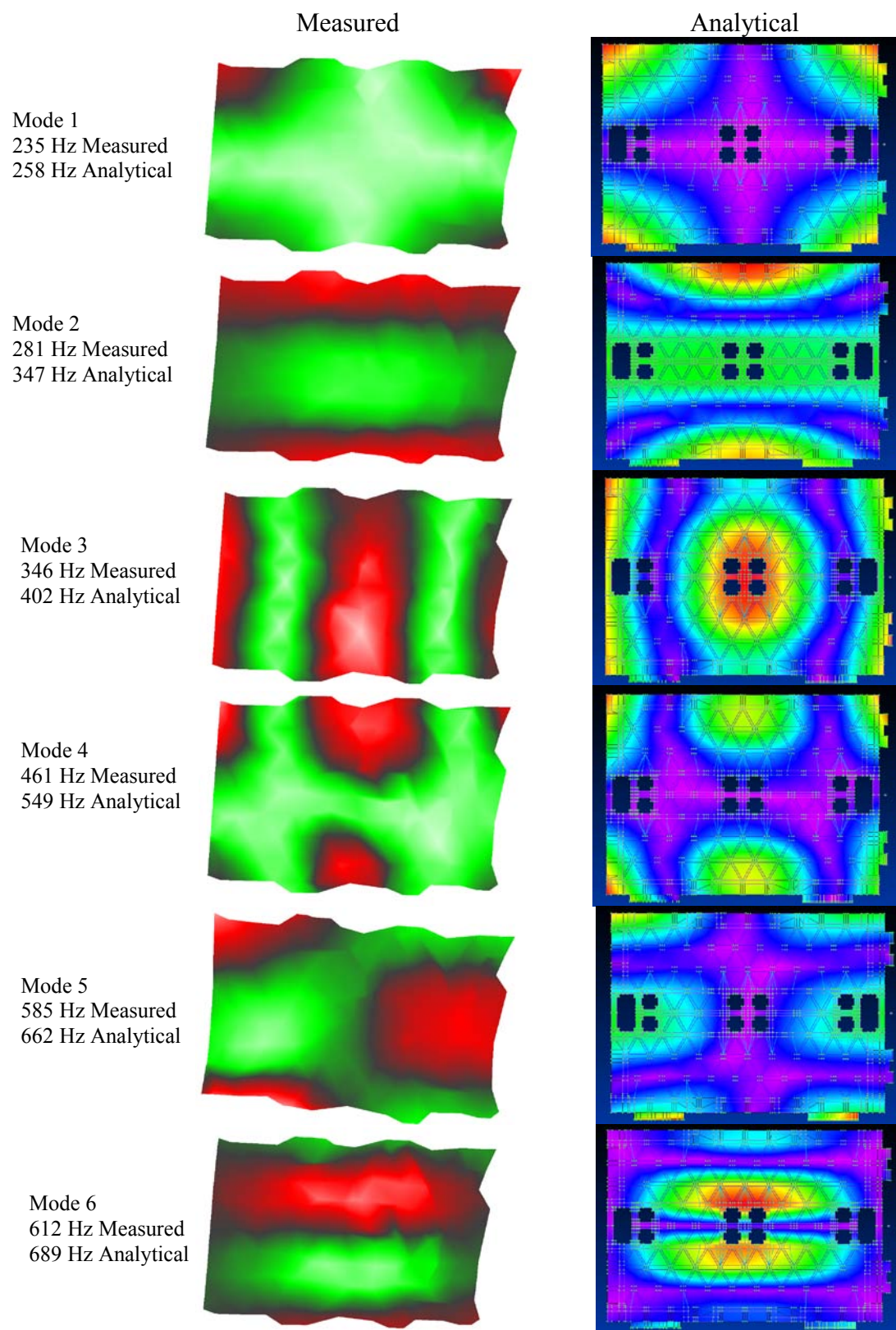


Figure 29: Measured versus analytical mode shapes –Y panel.

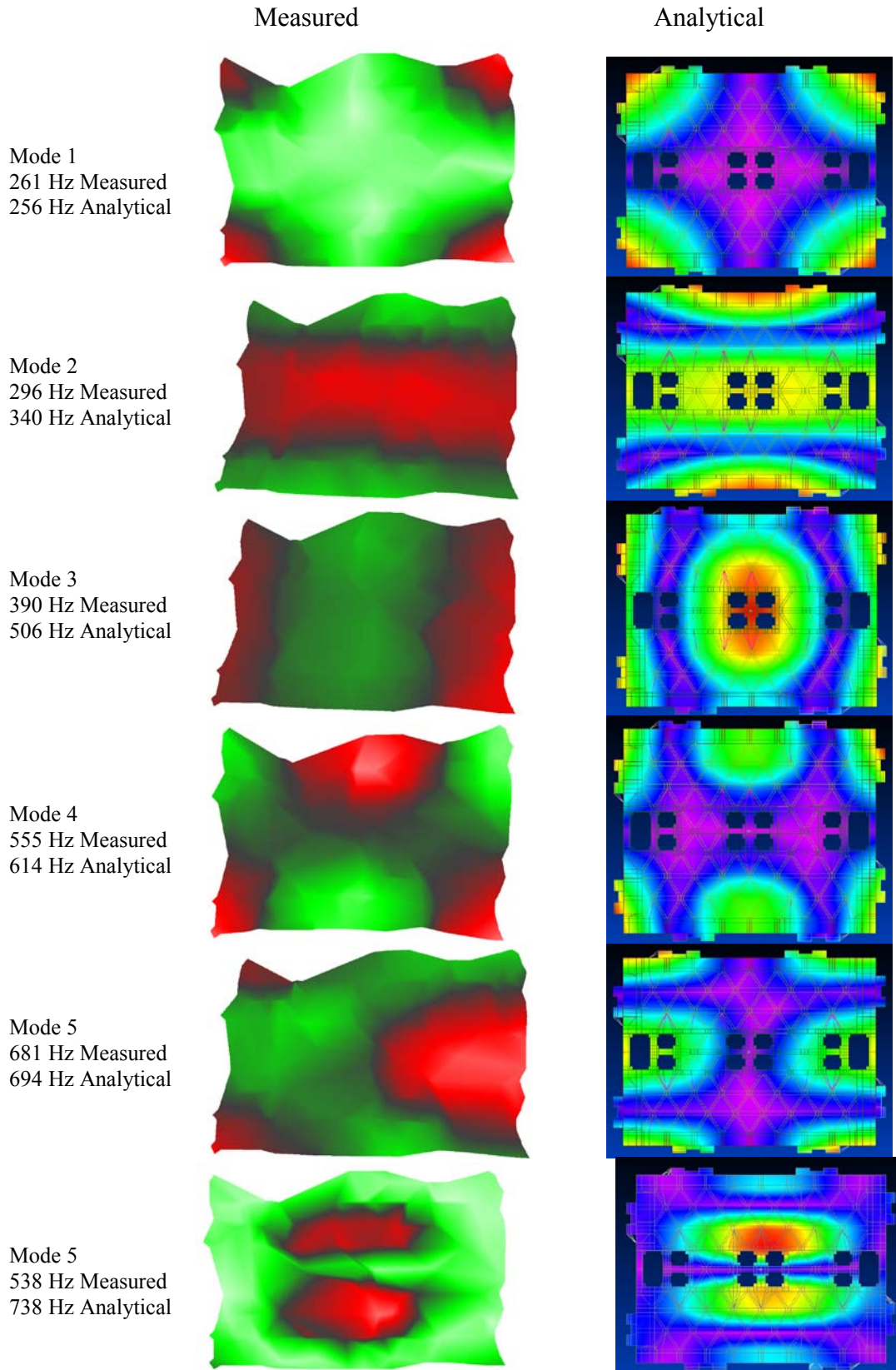


Figure 30: Measured versus analytical mode shapes –Z panel.

4.2 Tuned -Y and -Z panel FE model Results

The tuning process had to be re-accomplished several times to get acceptable results. First, there was an insufficient number of tuning parameters which resulted in failed tuning cases. It was necessary to go back into the FE model and increase the number of material cards present. Table 3 summarizes the before and after material cards

Table 3: Material cards -Z, -Y panels.

	-Z Panel	-Y Panel
Initial Material Cards	14	10
Final Material Cards	65	95

The objective function as written is very sensitive to small target values because the target values are in the denominator of J , these small values make the objective function erroneously large. This makes the tuning process very sensitive to only a few DOF in each mode. After discarding these data points with very small values and plotting the normalized untuned modes by the measured it became clear the objective function was absolved of these few bad data points. An example of a bad objective function and a correct objective function for the first mode of -Z panel can be seen in Figure 31.

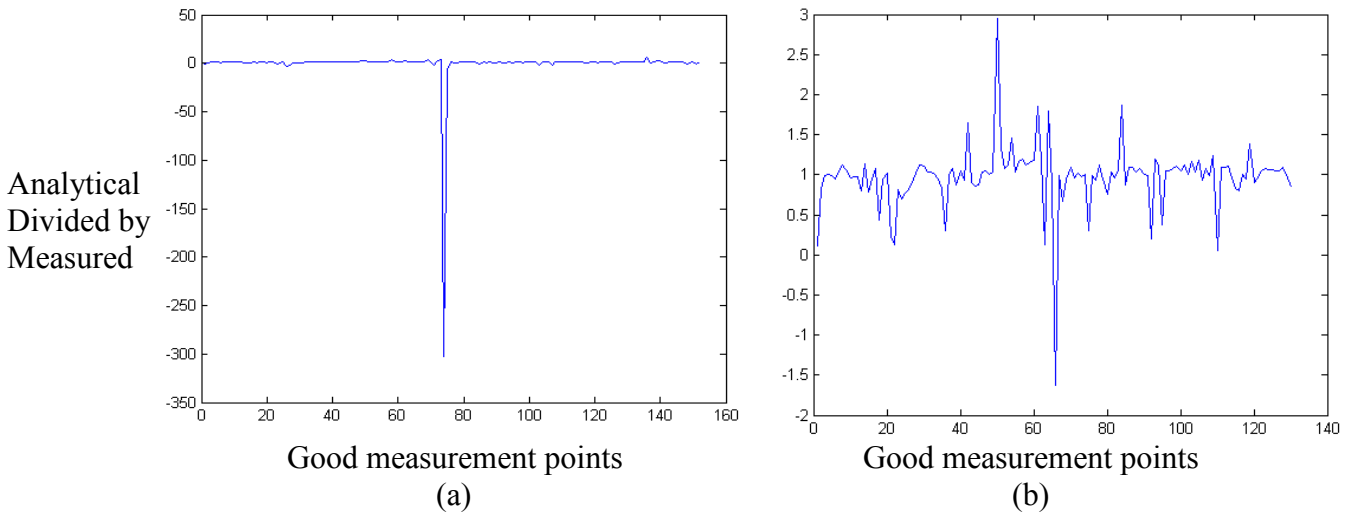
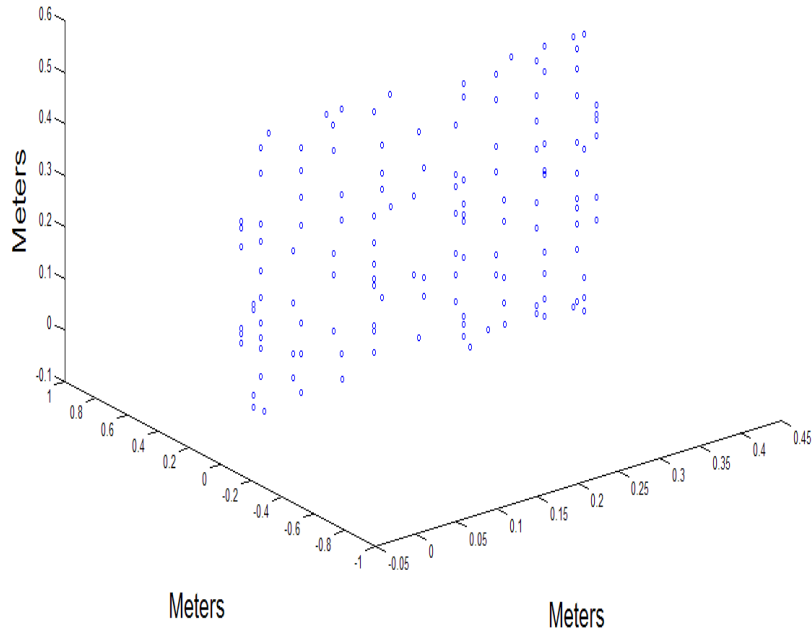
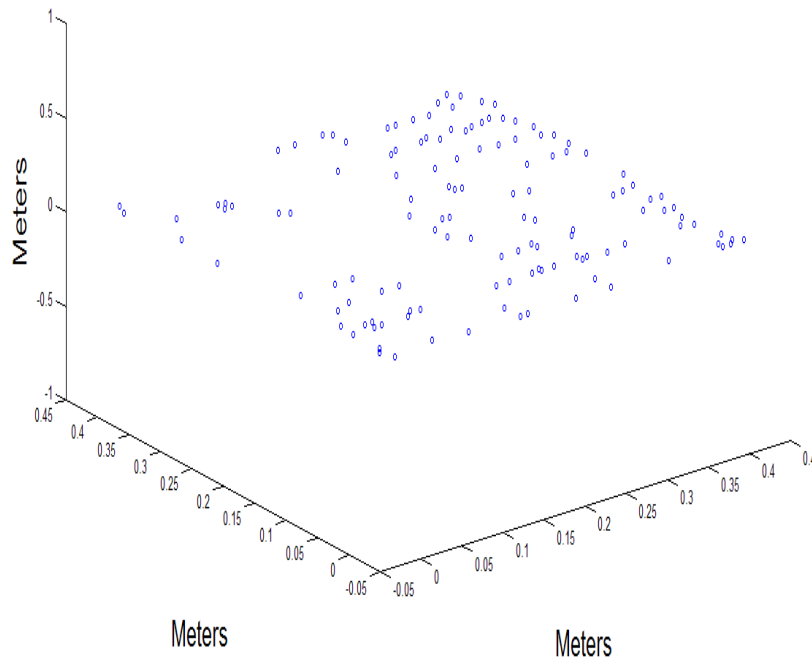


Figure 31: -Z Panel (a) Unsatisfactory objective function, single value approaching 300, tuned mode divided by small erroneous data (b) Removed bad data points all points with +/- 3 magnitude – note the y-axis scale difference.

With all the bad nodes removed, a visual check shows that all the nodes are in their correct locations and plane. There were 130 and 137 measurement locations in the $-Z$ and $-Y$ panels, respectively. The nodes being tuned are represented by circles in Figure 32:



(a)



(b)

Figure 32: (a) $-Z$ panel, 130 nodes (b) $-Y$ panel, 137 nodes.

Tuning results for the –Y and –Z panel are located in Table 4 and Table 5..

Table 4: Measured versus tuned for modes 1-6 for –Y panel.

			Measured vs Untuned		Measured vs Tuned
Mode	Measured (Hz)	Untuned (Hz)	Abs % Diff	Tuned (Hz)	Abs % Diff
1	235.4	258.0	9.60	229.5	2.51
2	281.6	347.0	23.22	289	2.63
3	346.1	402.0	16.15	348.8	0.78
4	461.3	549.0	19.01	472.8	2.49
5	585.2	662.0	13.12	574.9	1.76
6	612.2	689.0	12.54	597.6	2.38

Table 5: Measured versus tuned for modes 1-6 for –Z panel; ordered by analytical modes.

			Measured vs Untuned		Measured vs Tuned
Mode	Measured (Hz)	Untuned (Hz)	Abs % Diff	Tuned (Hz)	Abs % Diff
1	261.2	256.0	1.99	249.2	4.59
2	296	340.0	14.86	294.3	0.57
3	390	506.0	29.74	401.2	2.87
4	555.5	614.0	10.53	528.4	4.88
5	680.7	694.0	1.95	564.3	17.10
6	538	738.0	37.17	648.8	20.59

Observing Table 4 it is evident that –Y panel was tuned to be within +/- 3% of the measured data; however, the –Z panel proved much more difficult to tune. The FE model had modes in a different order than the measured data had them being shown. The 5th and 6th measured natural frequencies are 680.7 and 538 Hz, respectively. The measured and analytical modes agree in terms of order, but the tuning process had poor agreement with the frequencies. After comparing the frequencies it was important to look at the comparison between analytical and measured modes. Using a cross orthogonality check between the mass normalized measured and tuned eigenvectors we arrive at a value from 0 to 1, 1 being nominal. A comparison of the measured versus measured, and measured versus tuned are in Figure 33 with a comparison of the cross-

orthogonality terms in Table 6. The comparison is done using a mass weighted orthogonality check. Given as Eq. (26) were M_{AA} is the Guyan reduced mass matrix.

$$XO_{ij} = \phi_{iA}^T M_{AA} \phi_{jM} \quad (26)$$

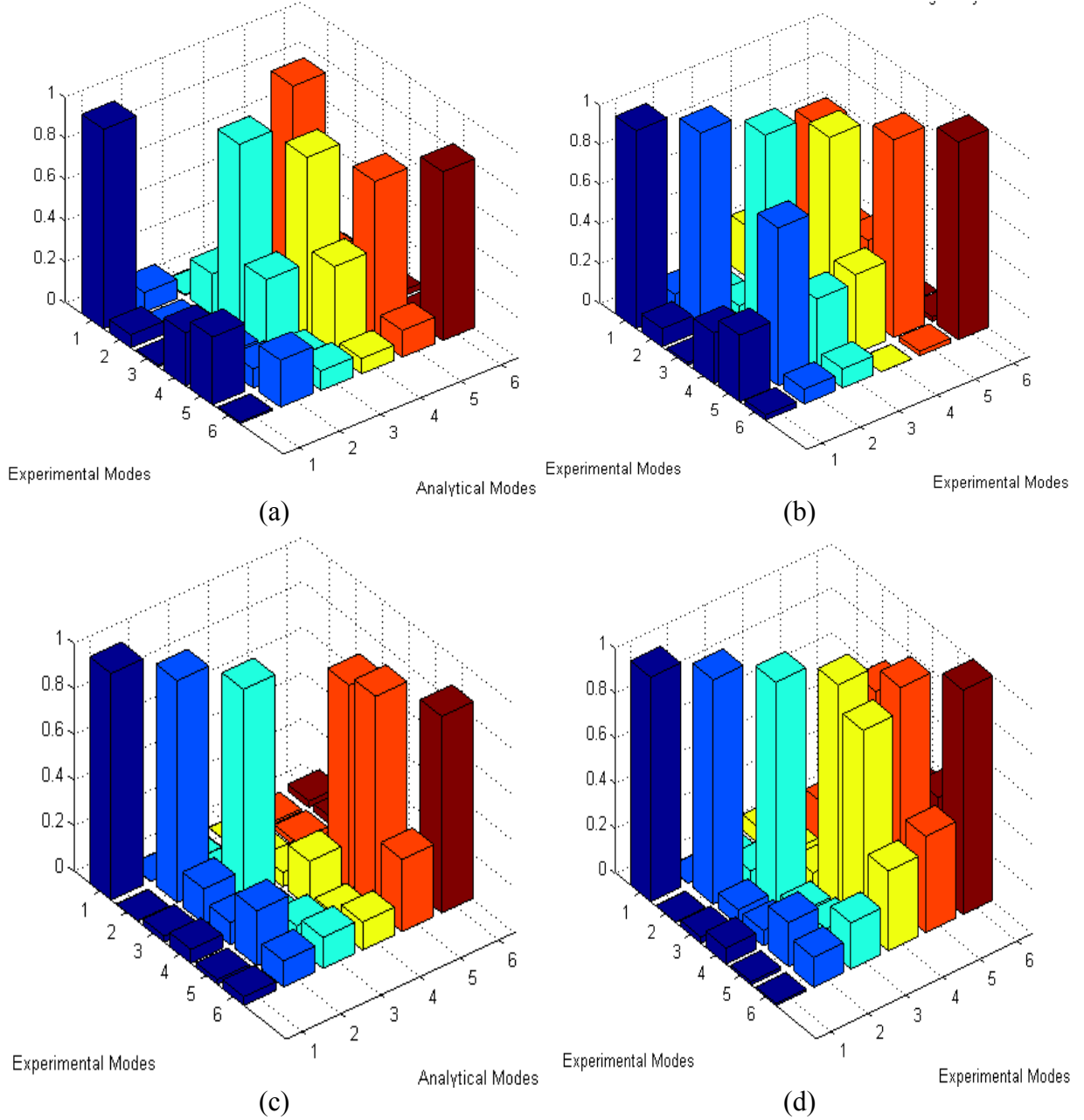


Figure 33: (a) -Y panel tuned cross-orthogonality results (b) -Y measured vs. measured cross-orthogonality (c) -Z panel tuned cross-orthogonality results (d) -Z measured vs. measured cross-orthogonality

Table 6: Table comparing untuned and tuned cross orthogonality checks –Z panel.

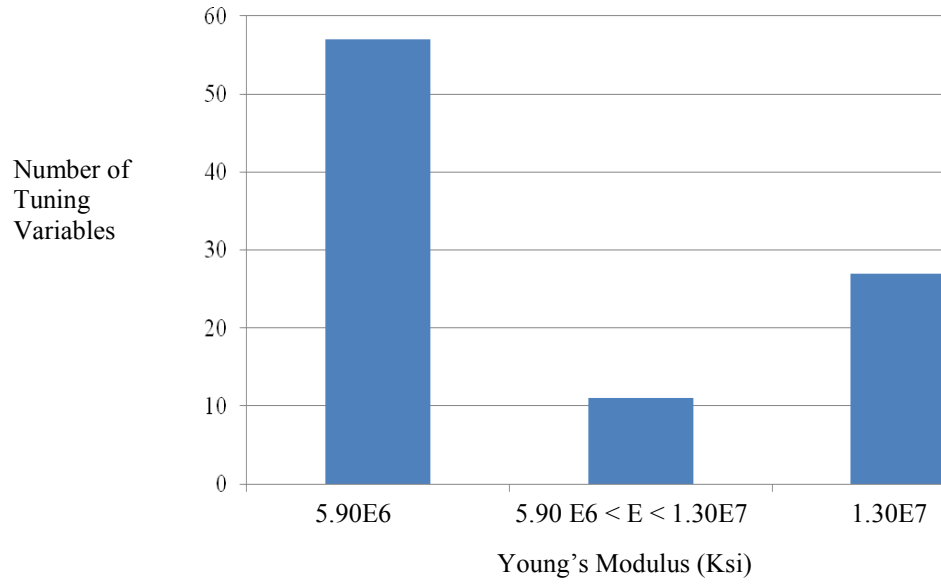
Mode #	X0 Untuned	X0 Tuned
1	0.995	0.996
2	0.970	0.976
3	0.935	0.949
4	0.200	0.204
5	0.937	0.941
6	0.895	0.865

Table 7: Table comparing untuned and tuned cross orthogonality checks –Y panel.

Mode #	X0 Untuned	X0 Tuned
1	0.977	0.973
2	0.947	0.229
3	0.929	0.923
4	0.895	0.870
5	0.102	0.952
6	0.879	0.822

Observing the measured versus measured cross orthogonality plots it is important to notice the similarities between the 4th and 5th mode for the -Z panel and the 2nd and 5th mode for the -Y panel. For each panel the similarities that exist are noticeable on the cross orthogonality plots. These modes being so closely aligned affect the tuning ability because the optimization process has difficulty determining the difference between these modes.

A brief look at the tuned Young's moduli for the –Y and –Z panel are shown in Figure 34 and Figure 35, respectively. The initial value of the Young's moduli for both models was 9.9E6 Ksi.



(a)

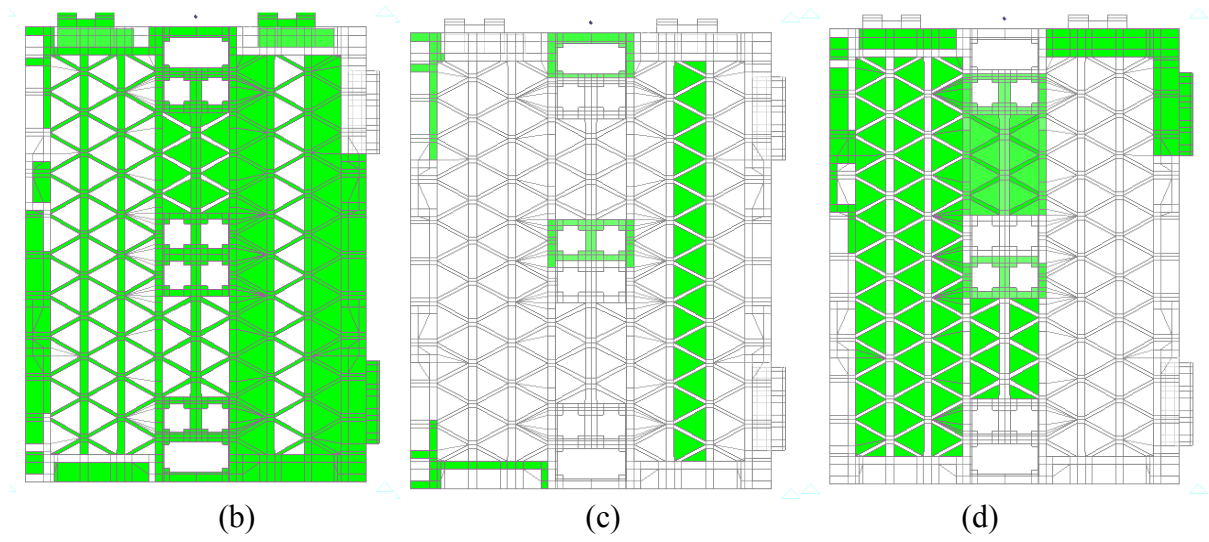
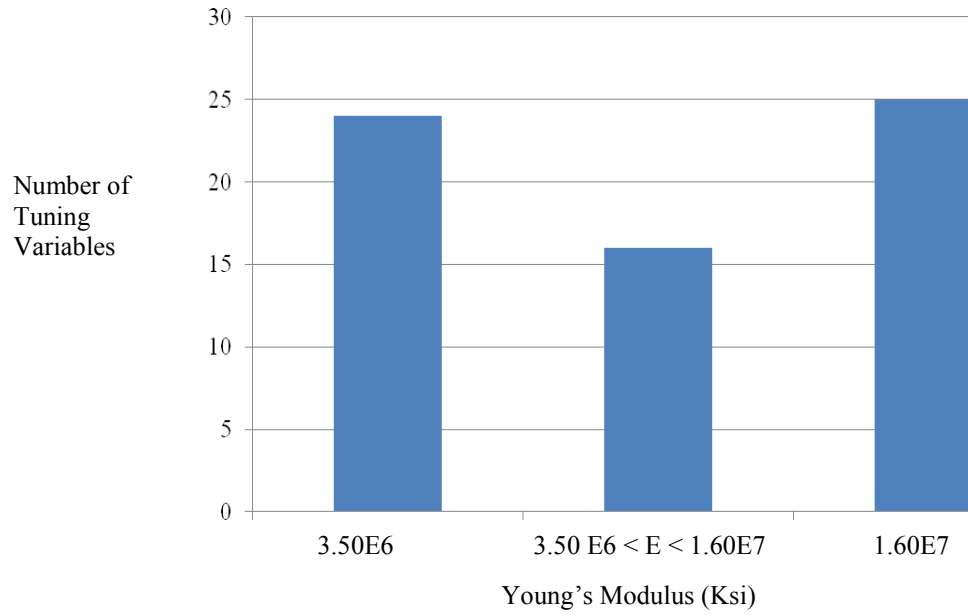
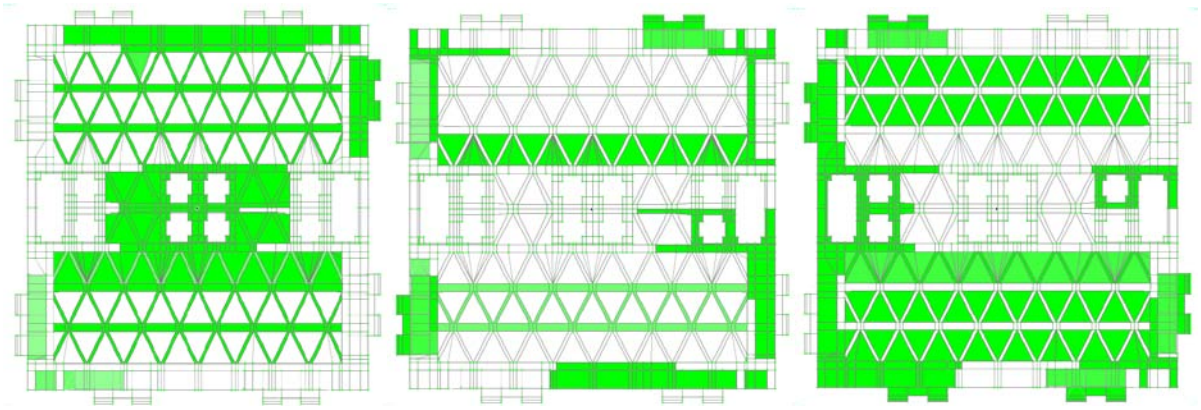


Figure 34: (a) Modulus of Elasticity of the various tuning variables the -Y Panel. Initial value of 9.9E6 Ksi. (b) Elements with 5.90E6 modulus of elasticity. (c) Elements with modulus of elasticity between 5.90E6 Ksi and 1.30E7 Ksi. (d) Elements with modulus of elasticity of 1.30E7 Ksi.



(a)



(b)

(c)

(d)

Figure 35: (a) Modulus of Elasticity of the various tuning variables the -Z Panel. Initial value of 9.9E6 K si. (b) E lements w ith 3.50E 6 modulus of e lasticity. (c) E lements w ith m odulus of elasticity b etween 3.50E 6 K si a nd 1.60E 7 K si. (d) E lements w ith m o dulus o f e lasticity o f 1.60E7 Ksi.

4.3 Untuned PnPSAT I

The $-Y$ and $-Z$ panels described were chosen to represent the $-X$, $+X$, Y and Z , respectively, for the structure of PnPSAT I. The completed structure with components FE model was approximately six times smaller in size than the Spaceworks model. The difference in size can be seen in Table 8.

Table 8: Comparison of size of Spaceworks and reduced PnPSAT I FE models.

	Spaceworks PnPSAT I	Reduced PnPSAT I	Factor Smaller
Nodes	368,850	67,381	5.5
Elements	246,295	40,861	6.0
DOF	1,104,633	208,404	5.3

With PnPSAT I fully constructed the mass is validated to be within a 3% tolerance window. The actual mass of PnPSAT I was 113.143kg, the FE model was 115.854, this is a 2.4% difference; well within the tolerance limit. An eigenvalue and eigenvector analysis was conducted to ensure no localized modes or singularities exist before the tuning process began. The first natural frequency and mode shape analysis revealed the natural frequencies were too low and the base plate and $-Z$ panels were not adequately fastened with rigid links. Increasing the natural frequency was accomplished by conducting a coincident node check to rigidly attach the panels together. To fasten the base plate to the $-Z$ panel, more rigid links were added.

The parameters to be altered during the optimization process are the spring/dampers which attach the base plate and the adapter ring. This is justified because the panels have already been tuned and the base plate and adapter ring are the main sources of strain on the satellite. Looking at the strain energy for the first mode in Figure 36 it is evident that the Young's moduli and stiffness of the spring/dampers is most important during the complete PnPSAT I FE model tuning process.

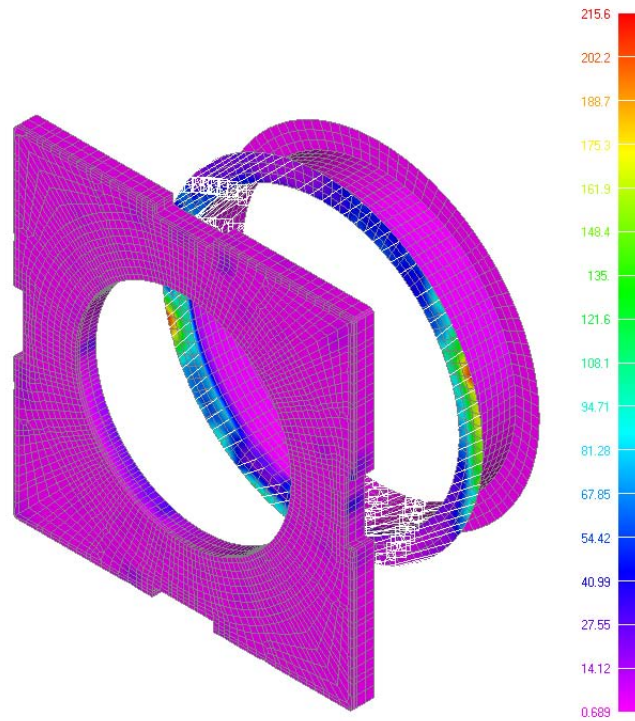
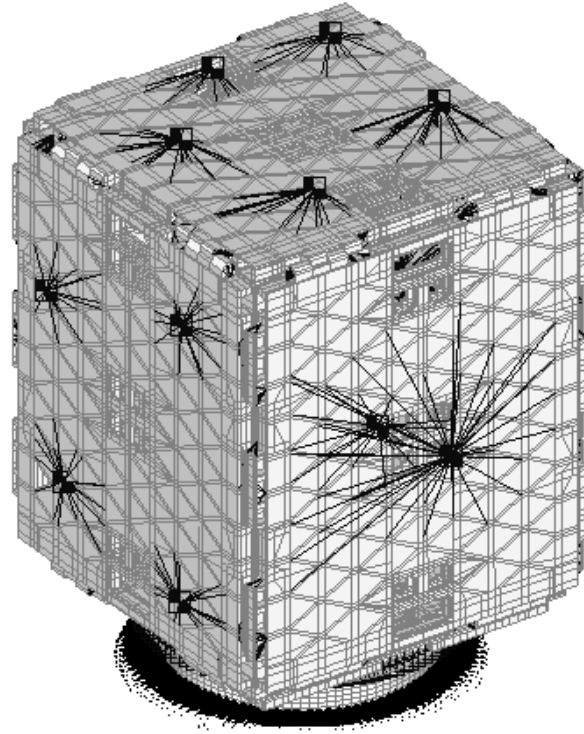
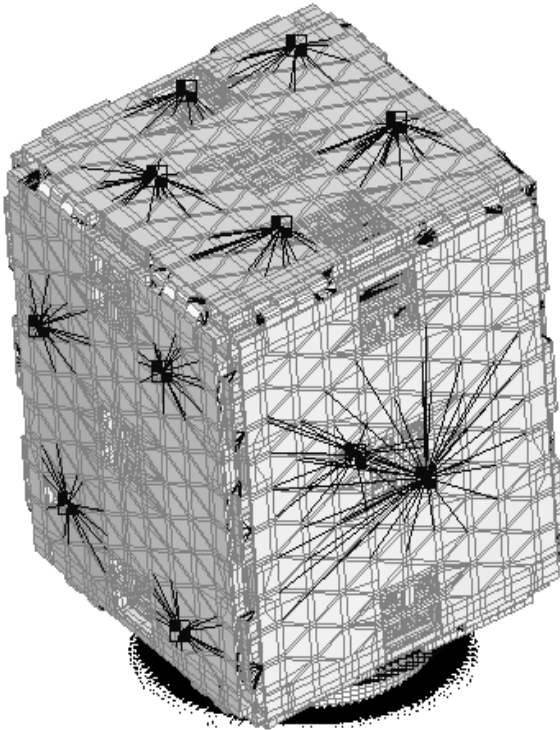


Figure 36: Blown up view between base plate and a dapter ring, primary strain along top of adapter ring.

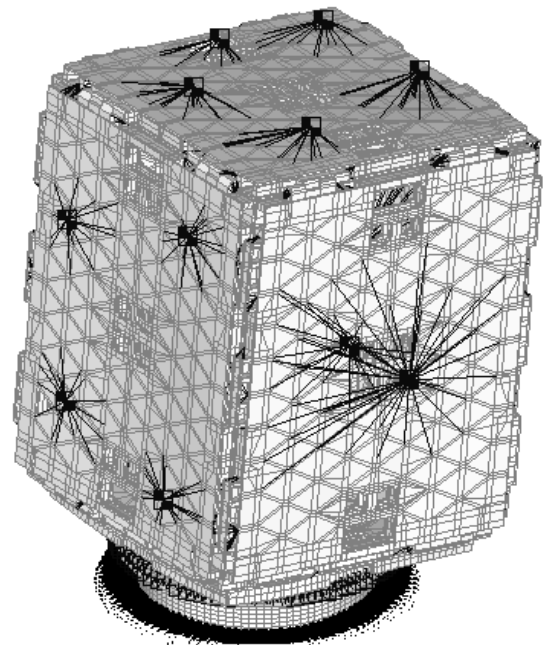
The initial stiffness values are allowed to change between a tolerance of .01% and 1000% of the starting value. The Young's moduli for the base plate and a dapter ring are allowed to be altered by up to +/-40% of the initial value. The first three modes and natural frequencies for the untuned PnPSAT I are seen in Figure 37, Figure 38, Figure 39.



(a)

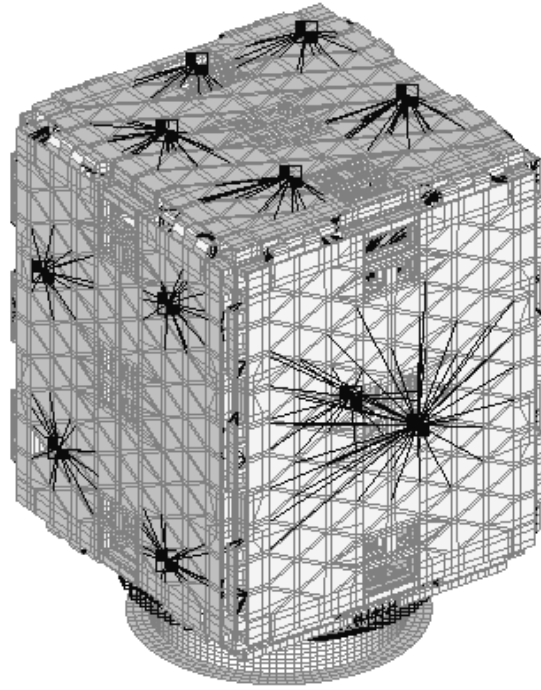


(b)

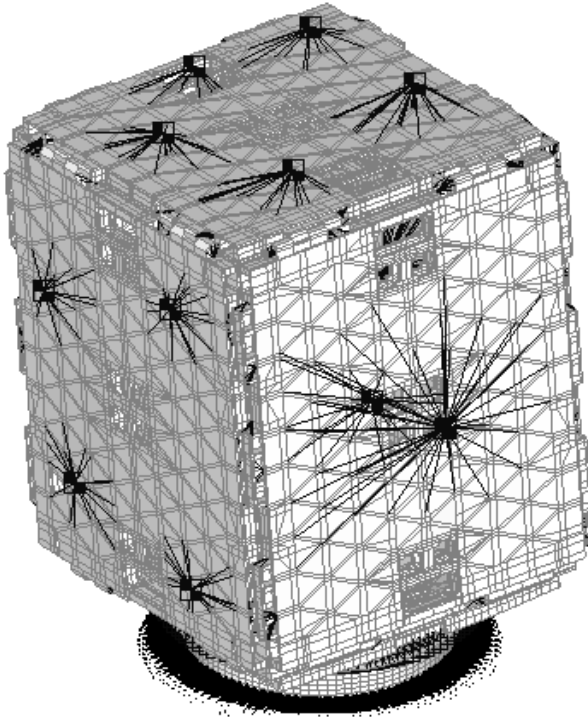


(c)

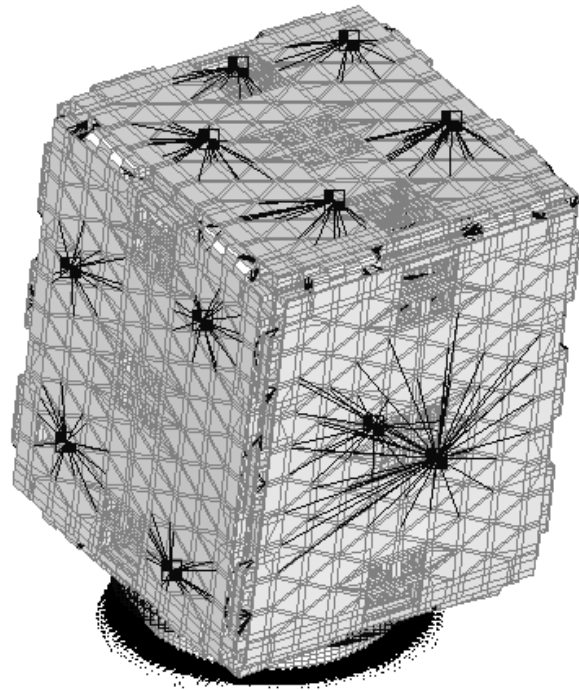
Figure 37: Mode 1: Rocking X: untuned 63.2 Hz: (a) undeformed dimetric view (b), (c) scaled up deflections demonstrating the rocking motion.



(a)

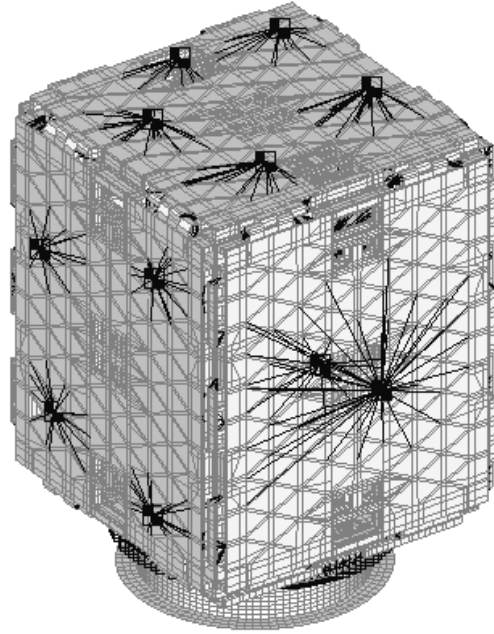


(b)

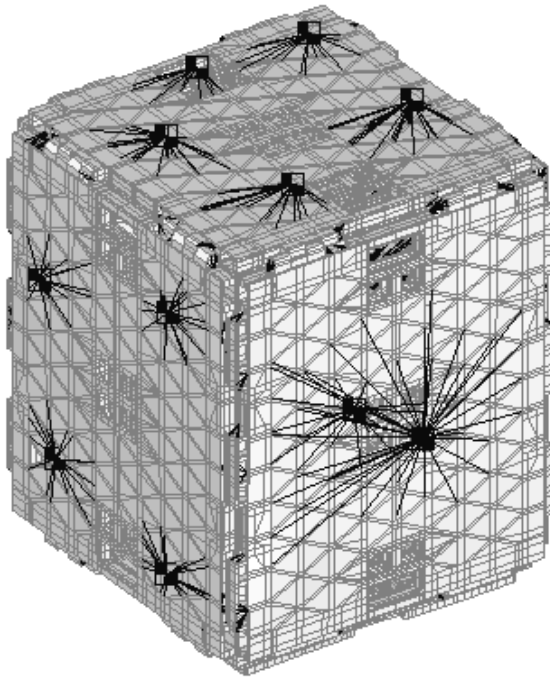


(c)

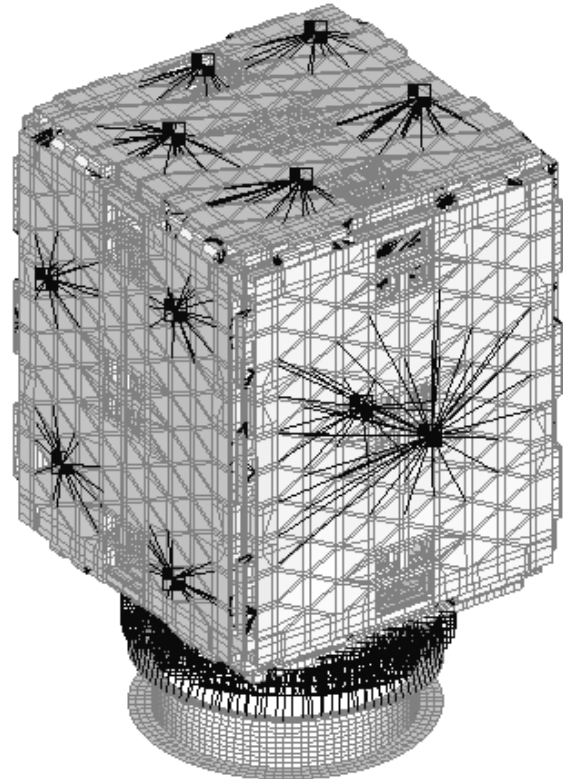
Figure 38: Mode 2: Rocking Y: untuned 70.6 Hz (a) undeformed dimetric view (b), (c) scaled up deflections demonstrating the rocking Y mode.



(a)



(b)



(c)

Figure 39: Mode 3: Pogo mode untuned 158.9 Hz (a) undeformed dimetric view (b), (c) scaled up deflections demonstrating the pogo mode.

4.4 Tuned PnPSAT I

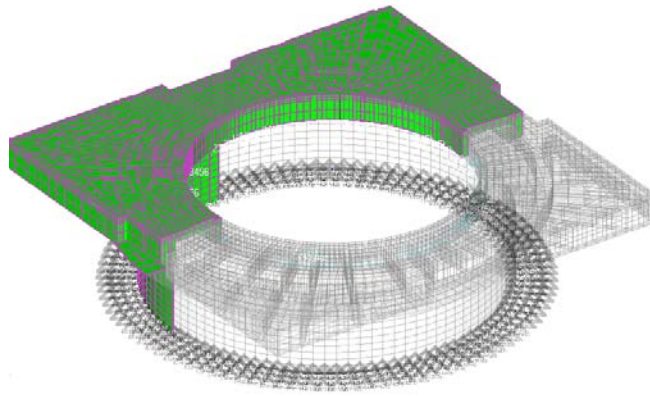
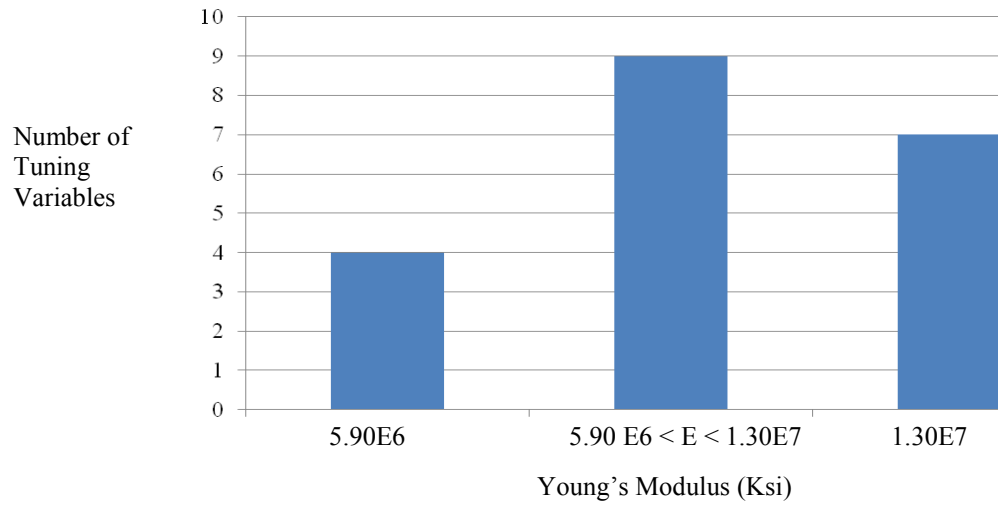
The tuning process for PnPSAT I was conducted with ease after the experience gained from tuning the $-Y$ and $-Z$ panels. The optimization process using 4 dual cores AMD 8200-2.8 GHz with 64 gigabytes of RAM took approximately 6 hours. The tuning process length grows based on n^3 operations, where n is the number of DOFs for the model. The Spaceworks model is approximately 6 times larger and the operations are cubed therefore making the total time per run unrealistically long.

The tuning process for PnPSAT I involved getting the natural frequencies for the first three modes to be within 5% of experimental data. A table summarizing the difference between the post tuned analytical and experimental is in Table 9.

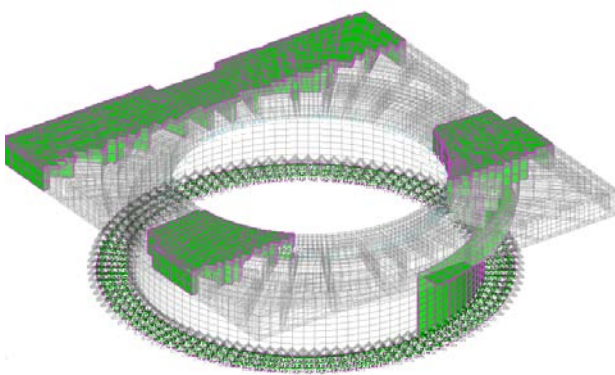
Table 9: Experimental vs. tuned natural frequencies for modes 1-3.

Mode	Measured (Hz)	Untuned (Hz)	Abs % Diff	Tuned PnPSAT I (Hz)	Abs % Diff
1	65.00	63.2	2.77	63.8	1.85
2	69.00	78.5	13.77	70.0	1.45
3	190.00	195.8	3.05	194.9	2.58

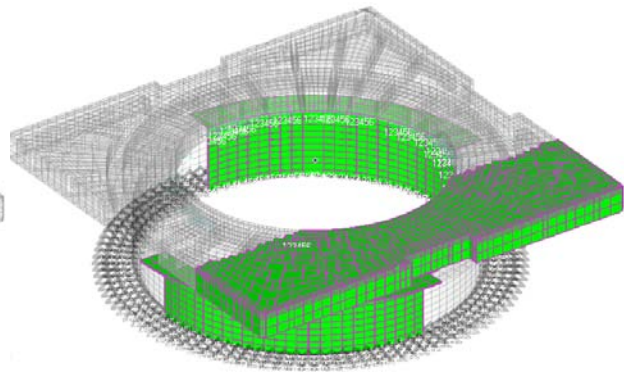
The table clearly shows the tuning process tuned the first three natural frequencies to within $\pm 3\%$ of the measured. The tuned Young's moduli values for the tuning variables are in Figure 40 while the spring stiffness coefficients are in Figure 41. Notice, the ceiling and floor were reached by several variables especially while tuning the springs.



(b)



(c)



(d)

Figure 40: (a) Modulus of Elasticity of the various tuning variables the -Y Panel. Initial value of 9.9E6 K si. (b) E lements w ith 5.90E 6 modulus of e lasticity. (c) E lements w ith m odulus of elasticity b etween 5.90E 6 K si a nd 1.30E 7 K si. (d) Elements w ith m o dulus o f e lasticity o f 1.30E7 Ksi.

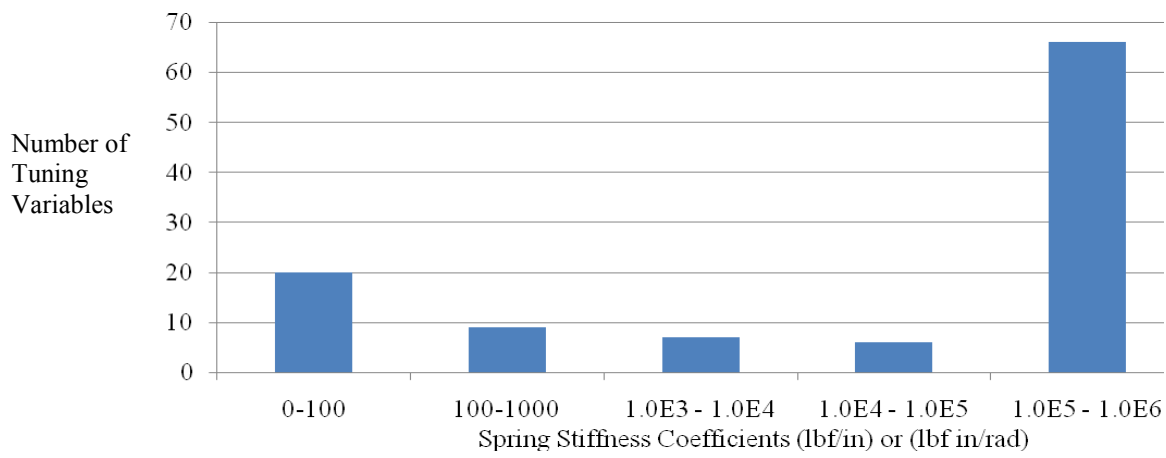


Figure 41: Spring Stiffness Coefficients: Includes both axial and torsional spring values. The initial starting parameter value was 1.0E3 lbf/in (axial) or 1.0E3 lbf in/rad (torisonal).

V. Conclusion

5.1 Research Overview

The PnP concept on which PnPSAT I was initially conceived is aimed at the elimination or minimization of expensive and time consuming AIT. The ORS goal is to launch payloads to space in only six days. The objective of this research is to investigate the possibility of creating an accurate FE model of PnPSAT I which can accurately predict the dynamic response of PnPSAT I.

In Chapter II, we discussed how to accomplish the process of creating an FE model, the methods used to extract frequency information from an object and the mathematical techniques used to conduct modal analysis. Also discussed was FE analysis which included, the assumptions implemented to create an FE model, modal analysis from the equations of motion (EOM) through the eigenvalue problem (EVP) leading to the modal frequency response problem. Lastly, the method used to extract data for tuning, PSV scanning LDV, and the objective function utilized for tuning the FE model with the acquired mode shapes and natural frequencies.

In Chapter III, we discussed how the original PnPSAT I FE model was created by Spaceworks and contained 1,104,633 DOFs. The size of this model made it extremely computationally expensive. A simple eigenvalue analysis on the model took 18 minutes on a dual core AMD 8 200-2.8GHz 64 gigabytes of RAM machine. The eigenvalue problem is solved thousands of times during the tuning process therefore the size of the PnPSAT I FE model needed to be reduced in order to allow the tuning process to finish in

a reasonable amount of time. The creation of a reduced FE model was started when the ORS office agreed to allow ping testing on the $-Y$ and $-Z$ panels. Assuming the $-X$, $+X$, Y and Z panels are the same as the $-Y$ and $-Z$ panels, respectively, it was possible to generate an accurate representation of PnPSAT I out of two correctly tuned panels. From this the geometry of the $-Y$ and $-Z$ panels were extracted from PnPSAT I's CAD file. A network of nodes was created by hand in FEMAP and meshed together by hand to create a fluid FE model for both the $-Y$ and $-Z$ panels.

Ping testing using the PSV scanning LDV was conducted to collect modes and natural frequencies for both the $-Y$ and $-Z$ panels. This was accomplished using an MB Dynamics Cal50 Exciter electrodynamic shaker being driven by a Hewlett Packard 33120A 15MHz/Arbitrary waveform generator programmed to generate a burst square wave to excite the panels. The tests provided excellent data in the lower frequencies, below ~ 500 Hz, with excellent coherence and spectral densities. The experimentally gathered data was then spectrally sieved using M E-Scope VES 5.0 to acquire clean averaged frequency response data. The tuning process involved ensuring analytical and experimentally gathered mode differences are minimized while ensuring the analytical and experimentally collected natural frequencies are held within their constraint limits of $\pm 5\%$.

The tuned panel models are copied and attached to create an initial structural FE model. The $-Z$ panel and base plate are rigidly attached via rigid links. The adapter ring and the base plate are attached via 6 DOF spring/damper elements. Lump masses with correct mass and moment of inertia in all three directions are rigidly attached to the structure leading to a complete PnPSAT I FE model. This complete FE model is tuned

once by ensuring the experimentally gathered and analytical natural frequencies are within $\pm 5\%$ of one another for the first three modes.

In Chapter IV, we discussed the $-Y$ and $-Z$ panels were 6.3 and 5.7 times smaller than the Spaceworks $-Y$ and $-Z$ panels respectively. The $-Y$ and $-Z$ panels were tuned to be within $\pm 5\%$ and 20% of the first six experimentally collected natural frequencies and modes, respectively. The Young's moduli were allowed to fluctuate up to $\pm 40\%$ of their original values. The $-Y$ panel was tuned within 3% for all six natural frequencies. The $-Y$ panel mode tuning are all within 20% with the exception of the 5th mode. The experimentally collected data for the 2nd and 5th mode are nearly the same. The tuning algorithm has difficulties discerning between the two therefore during the cross orthogonality checks the 2nd mode gets shoved down and the 5th mode is shoved up. The $-Z$ panel was tuned within 5% for the first 4 modes, the last two modes busted the constraint because the measured natural frequencies for the 5th and 6th mode are out of order with the FE model. The remedy for this was to swap the natural frequencies and modes in attempt for the tuning algorithm to adjust the models modes to the correct order. The tuning algorithm was not able to overcome this for the natural frequencies; however, the mode shapes do meet the 20% constraint with the exception of the 4th mode. In similar fashion as the $-Y$ panel the 4th and 5th mode are very similar to one another; hence why the 4th mode is not within the constraint limit.

The completed PnPSAT I model had approximately 6 times less DOF than the larger Spaceworks model. The PnPSAT I was tuned to be within $\pm 5\%$ of the first three experimentally collected natural frequencies. The Young's moduli of the base plate and the adapter ring were allowed to fluctuate up to $\pm 40\%$ of their original values. The

spring/damper element's stiffness varied from .01% to 1000% of their original values. The tuned PnPSAT I's FE model natural frequencies are all within in 3 % of the experimentally gathered data from KAFB tests.

5.2 Future Work

The ever changing and complex space community needs to be able to become faster and more agile in meeting demands. PnPSAT I provides excellent groundwork for studying the use of computationally inexpensive and accurate FE models in order to predict dynamic responses of various satellite configurations. Numerous additional tasks could be completed to further this research. First, studies could be focused on the effect of material cards on the tuning process, to include how many are ideal, what is an appropriate percentage the Young's modulus can change. Second, a look into the differences between performing a coincident node check versus using spring/damper elements to attach the panels and the relative effect of both on the tuning process. Third, a deeper look into a more effective way of connecting the point mass components to the satellite should be studied. The use of rigid links is somewhat arbitrary and a study between different numbers of links and locations of links on stiffness should be explored. Fourth, research into the benefits of simply creating and tuning the entire PnPSAT I FE model initially; thereby, skipping the tuning process of individual panels. Lastly, experimentally collected natural frequencies and modal data could be acquired for the first 10 modes of the fully configured PnPSAT I. This information would drastically increase the confidence in the tuned PnPSAT I FE model. Using this tuned model it

would be possible to change the configuration of P nPSAT I and the FE model to determine if an accurately tuned structure can accurately predict dynamic solutions. This would help meet the ORS mission by allowing spacecraft engineers to possibly avoid AIT process all together and allow them to have full confidence in the FE model. This would ultimately benefit the ORS mission by reducing the time of AIT reducing the time it takes to get spacecraft on orbit to benefit the war fighter.

References

- Agilent, T. (2000), The fundamentals of modal testing, Tech. Rep. 5954-7957E, Agilent Technologies, telephone 1-800 452-4844.
- Allemang, R.J., "The Modal Assurance Criterion – Twenty Years of Use and Abuse," *Sound and Vibration*, Aug. 2003, pp. 14 – 23.
- Anderson, N., Robinson, G., and Newman, D., "Standardization to Optimize Integration and Testing", *3rd Responsive Space Conference*, Paper No. RS3-2005-4005, April 25–28, 2005, Los Angeles, CA.
- Babuska, V., Lacy, S.L., and L. Robertson, "On the Use of Multisine Input Signals for Plant Identification of Precision Structures," *48th AIAA/ASME/ASCH/AHS/ASC Structures, Structural Dynamics, and Materials Conference*, Honolulu, HI, Apr. 2007, AIAA Paper 2007-1794.
- Baghal, Lisa. "Assembly, Integration, and Test Methods for Operationally Responsive Space Satellites." Thesis. Air Force Institute of Technology, 2010. Print.
- Bhopale, Apoorva, and Charles J. Finley. "How ORS Will Answer the 7-Day." *7th Responsive Space Conference* (2009): 1-9. Print.
- Black, J., George, L., and Swenson, E. "Measuring and Modeling 3D Mode Shapes of FalconSAT-5 Structural Engineering Model," AIAA Paper 2008-1851.
- Caffin, M., Robinson, G., and Newman, D., "Remote Anywhere: Web-Based Spacecraft Integration and Checkout", *2nd Responsive Space Conference*, Paper No. RS2-2004-4004, April 19–22, 2004, Los Angeles, CA.]
- Calvi, A., "Uncertainty-based loads analysis for spacecraft: Finite element model validation and dynamic responses," *Computers and Structures*, Vol. 83, Issue 14, May 2005, pp. 1103-1112, doi:10.1016/j.compstruc.2004.11.019.
- Cobb, R.G., Canfield, R.A., and B.S. Liebst, "Finite Element Model Timing Using Automated Structural Optimization System Software," *AIAA Journal*, Vol. 34, No. 2, Feb. 1996, pp. 392-399.
- Coleman, Michelle, Chia-Yen Peng, and Kenneth Smith. "Test Verification of the Cassini spacecraft Dynamic Model." *IEEE Explore*. California Institute of Technology. Web.
- Cook, R. D., D. S. Malkus, M. E. Plesha, and R. J. Witt (2002), *Concepts and Applications of Finite Element Analysis*, 719 pp., John Wiley and Sons, INC.

de Klerk, D., and S.N. Voormeeren, "Fine-Tuned Vehicle Components: Using the 3-D Scanning Vibrometer to Validate a Real-Axle-Carrier FEM Model," InFocus Optical Measurement Solutions, Polytec, Issue 02, 2007, pp. 5-7.

Doupe, C., Swenson, E., George, L., and Black, J. "Finite Element Model Tuning with 3D Mode Shapes from FalconSAT-5," 50th AIAA/ASME/ASCE/AHS/ASC Structures, Structural Dynamics, and Materials Conference, May 2008.

Flanigan, Christopher C. "Implementation of the IRS Dynamic Reduction Method in MSC/NASTRAN." *1990 MSC/NASTRAN World Users Conference* (1990).

Friswell, M. L., and J. E. Mottershead (1995), *Finite Element Model Updating in Structural Dynamics*, 286 pp., Kluwer Academic Publishers, Boston.

Friswell, M. L., and J. E. Mottershead, *Finite Element Model Updating in Structural Dynamics*, Kluwer Academic, Boston, 1995, ISBN 0-7923-3431-0.

Fronterhouse, Don, Ken Center, and Jeff Preble. "Building SPA PnP Satellites." *7th Responsive Space Conference* (2009): 1-7. Print.

Gooding, J.C., Babuska, V., Griffith, D.T., Ingram, B.R., and L.M. Robertson, "Study of Free-Free Beam Structural Dynamics Perturbations due to Mounted Cable Harnesses," 48th AIAA/ASME/ASCE/AHS/ASC Structures, Structural Dynamics, and Materials Conference, Honolulu, HI, Apr. 2007, AIAA Paper 2007-2390.

Juang, J., and Pappa, R. S., "An Eigensystem Realization Algorithm for Modal Parameter Identification and Model Reduction," *Journal of Guidance, Control, and Dynamics*, Vol. 8, No. 5, 1985, pp. 620-627.

Kammer, D. C. and A. D. Steltzner, "Structural Identification using Inverse System Dynamics," 17th International Modal Analysis Conference, Kissimmee, FL, SEM, 1999, pp. 1880-1886.

Lacy, S.L., Babuska, V., Schrader, K.N., and R. Fuentes, "System Identification of Space Structures," Proceedings of the 2005 American Control Conference, Portland, OR, June 2005, pp. 2335-2340.

Lane, S., Lacy S., Babuska, and Carter, D., "Correlation and Error Metrics for Plant Identification of On-Orbit Space Structures," *Journal of Spacecraft and Rockets*, Vol. 44, No. 3, May-June 2007.

Marco-Gomez, V., Lopez-Diez, J., and P. Luengo, "Finite Element Model of a Large Spacecraft Structure Updated with Modal Test," AIAA Paper 99-1452.

MIL- HDBK- 340A (USAF), Do D HAND BOOK T EST R EQUIREMENTS F OR LAUNCH, UPPER-STAGE, AND SPACE VEHICLES, Vol I : Baselines, 01 April 1999.

Modak, S .V., K undra, T.K., a nd B .C. N akra, “Sudies in D ynamic D esign U sing Updated Models” Journal of Sound and Vibration, Vol. 281, Issues 3-5, Mar. 2005, pp. 943-964, doi:10.1016/j.jsv.2004.02.056.

Niedbal, N ., “ Analytical D etermination of R eal N ormal M odes f rom M easured Complex Responses,” AIAA Paper 1984-0995.

Richardson, M. H. (1997), Is it a mode shape or an operating deflection shape.

Robertson, L.M., Lane, S.A., Ingram, B.R., Hansen, E.J., Babuska, V., Gooding, J., Mimovich, M ., M ehle, G ., C oombs, D ., a nd E .V. A rdelean, “ Cable E ffects on t he Dynamics o f Large Precision S tructures,” 4 8th A IAA/ASME/ASCH/AHS/ASC Structures, S tructural Dynamics, a nd M aterials Conference, H onolulu, HI, A pr. 2007, AIAA Paper 2007-2389.

U.S. Air Force Research Lab Space Qualification Checklist

Wertz, J. and Larson, W ., ed., *Spacecraft Mission Analysis and Design (SMAD) III*, Microcosm Press, Kluwer Academic Publishers, 1999.

Yee, T ., “ Key E lements of R apid I ntegration a nd T est”, *3rd Responsive Space Conference*, Paper No. RS3-2005-4001, April 25–28, 2005, Los Angeles, CA.

REPORT DOCUMENTATION PAGE				Form Approved OMB No. 074-0188	
<p>The public reporting burden for this collection of information is estimated to average 1 hour per response, including the time for reviewing instructions, searching existing data sources, gathering and maintaining the data needed, and completing and reviewing the collection of information. Send comments regarding this burden estimate or any other aspect of the collection of information, including suggestions for reducing this burden to Department of Defense, Washington Headquarters Services, Directorate for Information Operations and Reports (0704-0188), 1215 Jefferson Davis Highway, Suite 1204, Arlington, VA 22202-4302. Respondents should be aware that notwithstanding any other provision of law, no person shall be subject to a penalty for failing to comply with a collection of information if it does not display a currently valid OMB control number.</p> <p>PLEASE DO NOT RETURN YOUR FORM TO THE ABOVE ADDRESS.</p>					
1. REPORT DATE (DD-MM-YYYY) 25-03-2010		2. REPORT TYPE Master's Thesis		3. DATES COVERED (From - To) March 2009 - March 2010	
TITLE AND SUBTITLE Accurate Dynamic Response Predictions of PnPSAT I				5a. CONTRACT NUMBER	
				5b. GRANT NUMBER	
				5c. PROGRAM ELEMENT NUMBER	
6. AUTHOR(S) Trottier, Michael D., 2d Lt, USAF				5d. PROJECT NUMBER	
				5e. TASK NUMBER	
				5f. WORK UNIT NUMBER	
7. PERFORMING ORGANIZATION NAMES(S) AND ADDRESS(S) Air Force Institute of Technology Graduate School of Engineering and Management (AFIT/ENY) 2950 Hobson Way, Building 640 WPAFB OH 45433-8865				8. PERFORMING ORGANIZATION REPORT NUMBER AFIT/GA/ENY/10-M12	
9. SPONSORING/MONITORING AGENCY NAME(S) AND ADDRESS(ES) Operationally Responsive Space 3550 Aberdeen Ave SE Bldg 592 Rm 58B Abq NM 263-6663 Charles.Finley@kirtland.af.mil Charles Finely				10. SPONSOR/MONITOR'S ACRONYM(S) ORS	
				11. SPONSOR/MONITOR'S REPORT NUMBER(S)	
12. DISTRIBUTION/AVAILABILITY STATEMENT APPROVED FOR PUBLIC RELEASE; DISTRIBUTION UNLIMITED.					
13. SUPPLEMENTARY NOTES					
14. ABSTRACT <p>Researchers at the Air Force Institute of Technology (AFIT) and the Operationally Responsive Space (ORS) Office have conducted extensive vibration testing and structural modeling on the first ORS Plug-and-Play Satellite (PnPSAT I). The intent of this research effort is to evaluate the premise that current post-integration spacecraft environmental test requirements can be reduced or modified using accurately tuned finite element (FE) models. As part of this research, modal testing was conducted on the PnPSAT I structural panels at AFIT. The modal testing was part of a much larger series of experimental trials on various configurations of PnPSAT I at the Air Force Research Laboratory (AFRL) facilities at Kirtland Air Force Base (KAFB). Multiple sets of vibration data were also collected from accelerometers on PnPSAT I from standard and modified spacecraft prelaunch sine sweep and random vibration tests. The modal data collected at AFIT is used to tune two PnPSAT I panel FE models and the random vibration data collected at KAFB is used to tune the complete satellite for one configuration. The goal is to create an accurate FE model capable of predicting the dynamic response in a frequency range of 0 -300 Hz of various PnPSAT configurations. This modeling and tuning effort will be validated by comparing FE model predictions with measured vibrational response from the previously mentioned experimental trial.</p>					
15. SUBJECT TERMS Finite Element Model, Tuning, PnPSAT I, Laser Vibrometer, Doppler Effect, Structures, Vibrations					
16. SECURITY CLASSIFICATION OF:			17. LIMITATION OF ABSTRACT UU	18. NUMBER OF PAGES 93	19a. NAME OF RESPONSIBLE PERSON Eirc D. Swenson, Lt Col, USAF ADVISOR
a. REPORT U	b. ABSTRACT U	c. THIS PAGE U			19b. TELEPHONE NUMBER (Include area code) (937) 255-6565, ext 7479 (Eric.Swenson@afit.edu)

Standard Form 298 (Rev. 8-98)
Prescribed by ANSI Std. Z39-18